JOURNAL OF GEOPHYSICAL RESEARCH, VOL. 112, D10111, doi:10.1029/2006JD007859, 2007

A tropospheric assessment of the ERA-40, NCEP, and JRA-25 global reanalyses in the polar regions

David H. Bromwich,[1,2] Ryan L. Fogt,[1,2] Kevin I. Hodges,[3] and John E. Walsh[4]

Received 31 July 2006; revised 17 November 2006; accepted 21 November 2006; published 22 May 2007.

[1] The reliability of the global reanalyses in the polar regions is investigated. The overview stems from an April 2006 Scientific Committee on Antarctic Research (SCAR) workshop on the performance of global reanalyses in high latitudes held at the British Antarctic Survey. Overall, the skill is much higher in the Arctic than the Antarctic, where the reanalyses are only reliable in the summer months prior to the modern satellite era. In the Antarctic, large circulation differences between the reanalyses are found primarily before 1979, when vast quantities of satellite sounding data started to be assimilated. Specifically for ERA-40, this data discontinuity creates a marked jump in Antarctic snow accumulation, especially at high elevations. In the Arctic, the largest differences are related to the reanalyses' depiction of clouds and their associated radiation impacts; ERA-40 captures the cloud variability much better than NCEP1 and JRA-25, but the ERA-40 and JRA-25 clouds are too optically thin for shortwave radiation. To further contrast the reanalyses skill, cyclone tracking results are presented. In the Southern Hemisphere, cyclonic activity is markedly different between the reanalyses, where there are few matched cyclones prior to 1979. In comparison, only some of the weaker cyclones are not matched in the Northern Hemisphere from 1958–2001, again indicating the superior skill in this hemisphere. Although this manuscript focuses on deficiencies in the reanalyses, it is important to note that they are a powerful tool for climate studies in both polar regions when used with a recognition of their limitations.

Citation: Bromwich, D. H., R. L. Fogt, K. I. Hodges, and J. E. Walsh (2007), A tropospheric assessment of the ERA-40, NCEP, and JRA-25 global reanalyses in the polar regions, *J. Geophys. Res.*, *112*, D10111, doi:10.1029/2006JD007859.

1. Introduction

[2] In the polar regions, it is difficult to place current weather and climate trends in a long-term climatological perspective, mostly because the meteorological records in these areas are spatially sparse and short in comparison with other regions of the globe. The low spatial density of polar meteorological data makes it challenging to separate local changes from regional or even continental-scale changes, especially in Antarctica, where the data density is the lowest. To help solve the problem of discontinuous, spatially incomplete meteorological records in these regions and across the globe, global reanalyses were developed in which a fixed assimilation scheme is used to incorporate past observations into an atmospheric numerical weather prediction model. As such, a reanalysis produces a large number of variables on a uniformly spaced grid. The National Aeronautics and Space Administration (NASA) Data Assimilation Office (DAO) created the first-ever global reanalysis, spanning 1979–1993 [*Schubert et al.*, 1993]. However, this reanalysis did not receive much attention or use, as soon after its release the National Centers for Environmental Prediction (NCEP) and the National Center for Atmospheric Research (NCAR) collaborated to produce the NCEP/NCAR global reanalysis (hereafter, NCEP1 [*Kalnay et al.*, 1996; *Kistler et al.*, 2001]). When it was first released, NCEP1 originally covered the period from 1948 to 1997, however, it is updated monthly by the Climate Data Assimilation System (CDAS) at NCEP to the present day. The longer time period of NCEP1 compared to the NASA DAO reanalysis is the primary reason why it has received much more use and attention.

[3] Since the release of NCEP1, other global reanalyses products have also been conducted and made available, namely the NCEP-Department of Energy Atmospheric Model Intercomparison Project2 (AMIP-2) reanalysis (NCEP2 [*Kanamitsu et al.*, 2002]), covering 1979 to present; the European Centre for Medium-Range Weather Forecasts (ECMWF) 15-year (ERA-15 [*Gibson et al.*, 1997, and references therein]) and 40-year reanalyses (ERA-40 [*Uppala et. al.*, 2005]), covering 1979–1993 and September 1957 to August 2002, respectively; and recently the Japan Meteorological Agency and Central Research

[1]Polar Meteorology Group, Byrd Polar Research Center, Ohio State University, Columbus, Ohio, USA.
[2]Atmospheric Sciences Program, Department of Geography, Ohio State University, Columbus, Ohio, USA.
[3]Environmental Systems Science Center, University of Reading, Reading, UK.
[4]International Arctic Research Center, University of Alaska-Fairbanks, Fairbanks, Alaska, USA.

0148-0227/07/2006JD007859$09.00

Table 1. Reanalysis Products Used in the Study[a]

Reanalysis	Time Period Covered	Horizontal Resolution	Number of Vertical Levels	Assimilation Method	Satellite Data Employed	Primary Sea Ice Determination	Snow Cover
NCEP1	1948–present	T62/ ~209 km	28	3D VAR	retrievals	GISST 1948–1978, SMMR and SSM/I 1979–present	NESDIS
NCEP2	1979–present	T62/ ~209 km	28	3D VAR	retrievals	SMMR and SSM/I	NESDIS
ERA-15	1979–1993	T106/ ~125 km	31	1D VAR	retrievals	SMMR and SSM/I	SYNOP
ERA-40	Sep 1957–Aug 2002	TL159/ ~125 km	60	3D VAR	radiances	HADISST1 1957–1981, then Reynolds OI	SYNOP
JRA-25	1979–2004	T106/ ~125 km	40	3D VAR	radiances	COBE	SSM/I and CPC/NCEP

[a]For sea ice, GISST = Global Sea Ice Cover and Sea Surface Temperature (SST) data; SMMR = Scanning Multichannel Microwave Radiometer; SSM/I = Special Sensor Microwave/Imager; HADISST1 = Hadley Centre Global Sea Ice Cover and SST data version 1 (replaced GISST); Reynolds OI = Reynolds optimally interpolated sea ice concentration; COBE = Centennial In Situ Observation-Based Estimates of the variability of SSTs and marine meteorological variables [*Ishii et al.*, 2005]. For snow cover, NESDIS = National Environmental Satellite, Data, and Information Service weekly analyses and climatology of snow cover; SYNOP = synoptic reports of snow depth; CPC/NCEP = Climate Prediction Center/NCEP weekly snow cover analysis.

Institute of Electric Power Industry 25-year reanalysis (JRA-25 [*Onogi et al.*, 2006]), covering the period 1979–2004. All of these products are available at a 2.5° by 2.5° resolution; higher-resolution data are also available with 1.875° by 1.875° resolution for NCEP1 and NCEP2, and 1.125° by 1.125° resolution for ERA-40 and JRA-25. At present, NCEP1, NCEP2, and JRA-25 are updated monthly, although ECMWF is currently conducting an update to the ERA-40 project with an interim global reanalysis at higher resolution using 4DVAR, spanning 1989 to present (Sakari Uppala, personal communication, 2006). Table 1 provides further details about these global reanalyses relevant to the polar regions.

[4] There are notable benefits of these reanalysis efforts. First, they each operate with a fixed assimilation system, so there are no changes in model physics or resolution (both horizontal and vertical) that may lead to spurious changes that may be erroneously identified as climate signals. Second, they are available globally at 6-hour intervals, which exceed the frequency of many routine polar observations, especially during their respective winter seasons. Third, the reanalyses are gridded products, thereby filling in large data voids. Fourth, the various reanalysis efforts include more quality controlled observations, which make them a much better tool for assessing climate change and variability in the poorly sampled polar regions than any available analyses. In most cases, the products are freely available and have thus had wide usage since their release [see, e.g., *Bromwich and Fogt*, 2004, and references therein]. Naturally, these benefits of reanalyses have greatly improved climate studies in the polar regions.

[5] However, with the continued use of these data sources, discoveries of their limitations in the high latitudes quickly were noticed. *Hines et al.* [2000] and *Marshall and Harangozo* [2000] found that there were large erroneous trends in winter mean sea level pressure (MSLP) and 500 hPa geopotential height fields in the Southern Ocean and near Antarctica in NCEP1 and NCEP2. These errors were related to the reanalyses' assimilation schemes in data sparse regions, which rejected observations because they did not align with the poor model climatology [e.g., *Bromwich and Fogt*, 2004]. As the data density increased, the model accepted more observations, which better constrained the result, but produced erroneous MSLP decreases in the circumpolar trough close to Antarctica. The bias in East Antarctica did not end until the mid-1990s when many Australian automatic weather stations were assimilated into NCEP1/2 [*Hines et al.*, 2000; *Marshall and Harangozo*, 2000; *Marshall*, 2002; *Bromwich and Fogt*, 2004]. Additionally, there was a problem in assimilating bogus pressure observations in NCEP1 (the PAOBS problem, see online at http://www.cpc.ncep.noaa.gov/products/ wesley/paobs/paobs.html) which affects the reanalysis in the 40°–60°S band on daily to weekly timescales.

[6] A comprehensive study of the performance of NCEP1 and ERA-40 across the middle and high latitudes of the Southern Hemisphere was conducted by *Bromwich and Fogt* [2004]. Their results show that ERA-40 displays strong trends in the correlation between observations and reanalyses values with time related to the assimilation of greater quantities of satellite data, with excellent skill attained during the modern satellite era (1979–2001). *Renwick* [2004] and *Trenberth et al.* [2005] reach similar conclusions on the quality of ERA-40, which led *Trenberth et al.* [2005] to correct the ERA-40 surface pressure from 56°S to the Antarctic coast in order to make them reliable prior to 1979. These errors in both reanalyses are largest in the winter, due particularly to the decreased ship observations in coastal Antarctica during winter which help to constrain the reanalysis [cf. *Bromwich and Fogt*, 2004, Figures 2 and 9]. Therefore they conclude that neither ERA-40 nor NCEP1 are reliable prior to the modern satellite era for austral nonsummer climate studies across Antarctica and the Southern Ocean.

[7] In the Arctic, primarily due to larger quantities of data from the nearby populated land surfaces, the skill of the reanalyses hasn't been as compromised. *Trenberth and Smith* [2005] examined the conservation of dry air mass in ERA-40 as a method for validating the reanalysis. Not surprisingly, they found that this quantity was not conserved well in the Southern Ocean and across Antarctica prior to 1979, especially in the austral winter. However, in the Arctic, the dry air mass was nearly conserved throughout the full 1958–2001 time period. Additionally, only small surface pressure differences (1958–1972 compared with 1979–2001) in boreal winter existed over Greenland and Iceland; the rest of the high latitudes of the Northern Hemisphere showed small differences in winter as well as other seasons, very unlike the Southern Hemisphere. In addition, *Crochet* [2007] finds realistic Icelandic precipita-

tion in ERA-40 for all seasons spanning 1958–2002, although ERA-40 overestimates the frequency of precipitation occurrence, particularly in boreal winter. Despite the fact that the frequency is overestimated, the general agreement between ERA-40 precipitation and Iceland rain gauges suggest that ERA-40 throughout its full period reliably captures the intensity and position of the nearby Icelandic low, which governs precipitation in the region [e.g., *Hanna et al.*, 2004]. By extrapolation, this also implies that ERA-40 resolves the atmospheric general circulation in the North Atlantic with fidelity.

[8] Another study by *Bromwich and Wang* [2005] compared the NCEP1, ERA-15, and ERA-40 reanalyses with two independent rawinsonde data sets from the Arctic Ocean periphery in the late 1980s and early 1990s. Although they found large differences between the reanalyses upper level wind speeds and one of the rawinsonde archives, they concluded that the observations themselves were erroneous with roughly half of the actual values, contrary to the conclusions of *Francis* [2002]. They demonstrated that all the reanalyses they studied performed reliably for many tropospheric-state variables (i.e., geopotential height, wind speed and direction, temperature, humidity, precipitable water) for the edge of the Arctic Ocean during the modern satellite era. Although an extensive reanalysis validation over the full period in the Arctic has not yet been conducted, it is expected that the reanalyses' skill for the main circulation variables (pressure, geopotential height, and temperature) prior to the modern satellite era is likely to be much better than that derived from observational data by *Bromwich and Fogt* [2004] in the middle and high latitudes of the Southern Hemisphere.

[9] In April 2006, scientists from various international research organizations gathered at the British Antarctic Survey for a workshop funded by the Scientific Committee on Antarctic Research (SCAR) on the use and reliability of the long-term global reanalyses (NCEP1, NCEP2, ERA-40, and JRA-25) in the high latitudes. The workshop report is available online at http://ipo.npolar.no/reports/archive/reanalWS_apr2006.pdf. This paper synthesizes the results presented at this workshop for the benefit of the scientific community, so other researchers and reanalysis users may be aware of their limitations and successes in the low-to-middle troposphere in these meteorologically complex areas. As such, it provides many reanalysis assessments in the polar regions that are currently not available in the literature. The manuscript also evaluates the skill in the high latitudes of the most recent global reanalysis project, JRA-25. The paper is laid out as follows: Section 2 briefly describes the reanalysis products in more detail. Sections 3–5 describe recent assessments of these reanalyses in the Antarctic/Southern Ocean, the Arctic, and cyclonic variability in both regions, respectively. A summary and conclusions are reached in section 6.

2. Reanalysis Data

[10] An overview of the relevant characteristics for polar studies in each reanalysis is presented in Table 1. Although the reanalysis data are commonly available on a 2.5° by 2.5° degree grid every six hours, the models are run at higher resolutions (TL159/∼125 km for ERA-40 and T62/209 km for NCEP1-2) and downgraded to a 2.5° resolution. ERA-40 contains 60 vertical levels (23 standard pressure levels) compared to the 28 vertical levels (17 standard pressure levels) of NCEP1, and is based on a "linear-grid" option mode, which helps to reduce spectral ripples (the Gibbs phenomenon) in the model orography over the oceans or flat land close to mountain ranges [*Uppala et al.*, 2005]. The model resolution for JRA-25 is approximately equivalent to ERA-40, T106/∼125 km, with 40 vertical levels (23 standard pressure levels). This is also the same as in ERA-15, which is mentioned only occasionally in this assessment due to its temporal shortness. All the reanalyses use three-dimensional variational assimilation (3D VAR) schemes except ERA-15, which is based on 1D VAR.

[11] Raw satellite radiances are assimilated into ERA-40, compared to the use of satellite retrievals by the NCEP series of reanalyses. Retrievals estimate the vertical temperature and humidity profiles through a series of empirical and statistical relationships, while raw radiances are direct measurements of atmospheric radiation acquired by the satellite sensors. Incorporating raw radiances requires more computational time and power, but eliminates the errors associated in the retrieval process. ERA-40 contains greater quantities of earlier satellite data from the Vertical Temperature Profile Radiometer (VTPR) starting in 1973 than those from NCEP1, which helped to better constrain ERA-40 prior to the assimilation of the TIROS Operational Vertical Sounder (TOVS) data in late 1978 [*Bromwich and Fogt*, 2004]. Various methods for determining the sea ice concentration and snow cover occur in the reanalyses.

[12] Notably, NCEP2 fixed errors in the snow cover in NCEP1 which repeatedly used the 1973 data for the entire 1974–1994 period [*Kanamitsu et al.*, 2002]. Two other relevant changes between NCEP1 and NCEP2 include fixing the PAOBS problem and removing the "spectral snow" problem in NCEP1 as displayed by *Cullather et al.* [2000]. NCEP1 is used primarily throughout the study, as most fields are very similar between the two reanalyses on the monthly and annual timescales employed here. Similarly, ERA-40 improved upon ERA-15 by fixing errors in the Antarctic orography and introducing the freezing of soil moisture and a land-cover dependent albedo for snow covered surfaces [*Uppala et al.*, 2005], while JRA-25 includes additional Chinese snow cover data that are not part of the other reanalyses [*Onogi et al.*, 2006]. Preliminary JRA-25 evaluations by K. Onogi et al. (The JRA-25 Reanalysis, submitted to *Journal of Meteorological Society of Japan*, 2007, hereinafter referred to as Onogi et al., submitted manuscript, 2007) demonstrate that the 500 hPa root mean square error in the Southern Hemisphere at 1979 is fairly consistent throughout the 1979–2004 period and comparable with the JMA global operational model at 1996, indicating the benefits of using a state-of-the-art assimilation scheme in conducting the JRA-25 reanalysis.

3. Evaluations in the Antarctic

[13] As noted in the Introduction, the main finding of *Bromwich and Fogt* [2004] in the middle and high latitudes of the Southern Hemisphere was that the ERA-40 and NCEP1 reanalyses are only reliable during the summer months prior to the start of the modern satellite era.

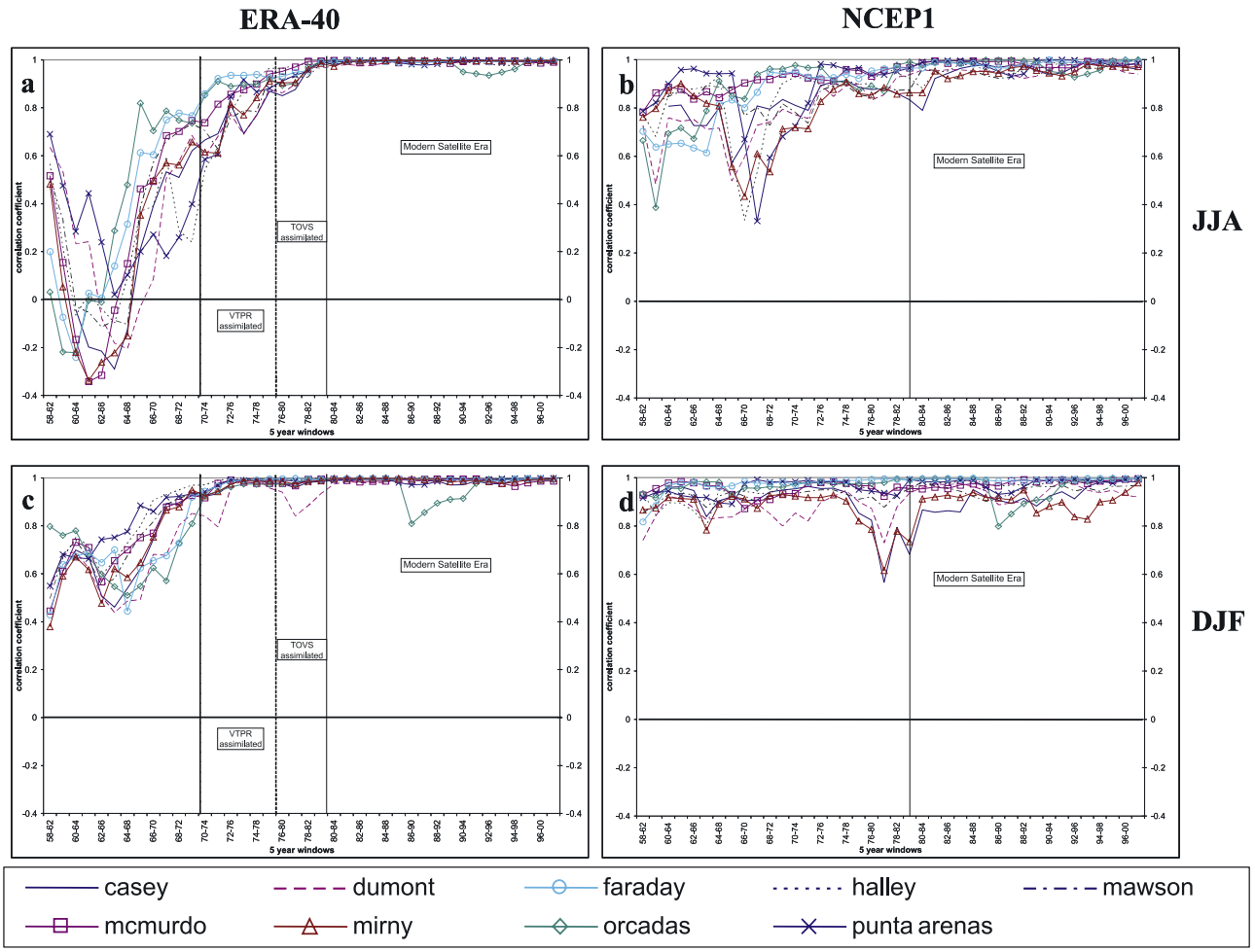

Figure 1. Five-year running mean sea level pressure (MSLP) correlations for (a) ERA-40 June-July-August (JJA), (b) NCEP1 JJA, (c) ERA-40 December-January-February (DJF), and (d) NCEP1 DJF compared to high southern latitude station observations. Adapted from *Bromwich and Fogt* [2004].

Although other variables (such as geopotential height and 2-m temperature) show strong seasonal changes in reanalysis skill, previous studies have demonstrated the notable effect that MSLP observations have on constraining the reanalysis [e.g., *Bromwich et al.*, 2000; *Hines et al.*, 2000; *Marshall and Harangozo*, 2000; *Marshall*, 2002] in data sparse regions, and thus only MSLP is presented here. Figures 1 and 2 examine the seasonal skill dependence in the reanalysis in greater detail by displaying the MSLP correlations of ERA-40 and NCEP1 compared with observations for austral winter (June-July-August (JJA), Figures 1a–1b) and summer (December-January-February (DJF), Figures 1c–1d), while Figure 2 presents the MSLP biases for both reanalyses in a similar fashion. As in the work of *Bromwich and Fogt* [2004], the results are shown in five year moving windows. Figures 1 and 2 clearly demonstrate that the skill is higher during the summer farther back into time, especially in NCEP1. In ERA-40, summer correlations (Figure 1c) are still relatively low before 1970 (the mean of the nine stations is 0.64 prior to 1970); however, these values are a significant improvement from the winter (Figure 1a) when the mean is 0.14. Notably in NCEP1, the winter biases (Figure 2b) are largest at the East Antarctic stations and smallest near the Antarctic Peninsula, but all regions are near zero during DJF (Figure 2d). In comparison, the correlation errors are spatially uniform in ERA-40 for both seasons (Figures 1a and 1c). The lower skill during the nonsummer months can be partly related to the handling of the early sea ice, as sea ice coverage strongly impacts atmospheric thermodynamics and thus the reanalysis performance. However, part of the error can also be attributed to the much smaller quantity of early ship observations during austral winter [cf. *Bromwich and Fogt*, 2004, Figure 9], which help to additionally constrain the reanalyses solution in the Southern Ocean. Thus both ERA-40 and NCEP1 perform well during the summer season in the high and middle latitudes of the Southern Hemisphere as the greater quantity of summer observations help to constrain the reanalysis, and there is much less dependence on accurately depicted sea ice coverage during austral summer.

[14] However, it is important to note that these checks are performed at places where station data are available. *Tennant* [2004] examines NCEP1 in the data sparse areas of the South Pacific and South Atlantic Oceans, and finds that even during the summer prior to 1979, NCEP1 frequently produces a weak meridional pressure/temperature

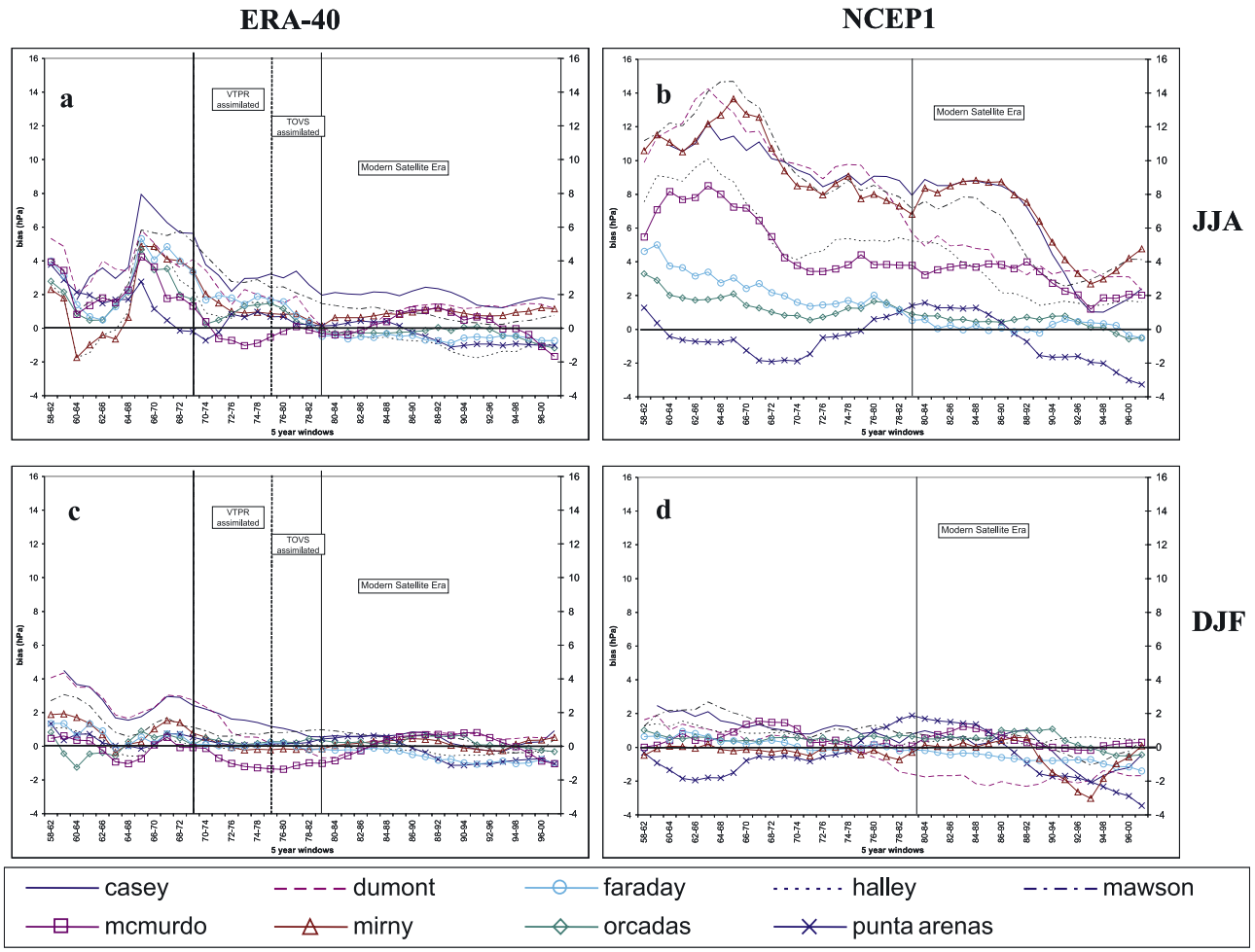

Figure 2. As in Figure 1 but for biases (hPa). Adapted from *Bromwich and Fogt* [2004].

gradient in these regions that is not observed as often in subsequent decades. He thus concludes that these patterns in NCEP1 are a reflection of its model climatology rather than reality, and therefore NCEP1 is not reliable during any season prior to 1979 in the Southern Hemisphere. However, because of marked decadal variability [*Fogt and Bromwich*, 2006] and the lack of observations in the regions studied by *Tennant* [2004], it is unclear exactly how well NCEP1 is performing during the austral summer in these specific locations, especially given its good skill with nearby available station data (Figures 1c–1d). Nonetheless, both *Bromwich and Fogt* [2004] and *Tennant* [2004] agree that in the nonsummer seasons prior to 1979, the reanalyses are primarily a reflection of their respective model climatology rather than reality in the Southern Hemisphere.

[15] To extend the analysis of *Bromwich and Fogt* [2004], the differences from 1979–2001 between the reanalyses 500 hPa geopotential height in the Southern Hemisphere are examined in Figure 3, including JRA-25. This level was chosen as it broadly represents the differences in the MSLP fields (Figures 1 and 2) due to the equivalent barotropic nature of the Antarctic atmosphere, and has the benefit of being the first mandatory pressure level that lies fully above the high Antarctic interior. Two key regions where the differences are the largest are seen in Figure 3: the interior of the Antarctic continent (Box 1; Figures 3b and 3c) and in the Southern Ocean off the East Antarctic coast (Box 2; Figure 3a). By averaging the 500 hPa geopotential heights for these regions (75°–85°S, 50°–130°E for Box 1 and 50°–60°S, 20°–50°E for Box 2), a time series is created that allows for the examination of the differences in more detail. Figure 4a presents the annual mean 500 hPa geopotential height averaged in Box 1, while Figure 4b displays annual mean averaged in Box 2 (note different vertical axes in Figures 4a and 4b). Figure 4a reveals that prior to 1998 NCEP1 displays a marked negative difference, although it does align with ERA-40 during 1989–1990, for unknown reasons. Better agreement is seen between ERA-40 and JRA-25, especially after 1991, coincident with the assimilation of the European Remote Sensing (ERS) Satellite altimeter data in ERA-40, although the agreement is likely not strongly influenced by this data and therefore the causality for this alignment remains uncertain. The sudden change in NCEP1 at 1998 is likely related to the assimilation of the Advanced TIROS Operational Vertical Sounder (ATOVS) data in this reanalysis, a microwave sounder not influenced with cloud clearing issues in the thermal infrared or visible spectrums, which thereby adjusted the height field over the Antarctic continent in NCEP1. The differences in Box 2 (Figure 4b) are less distinct, however it is seen that

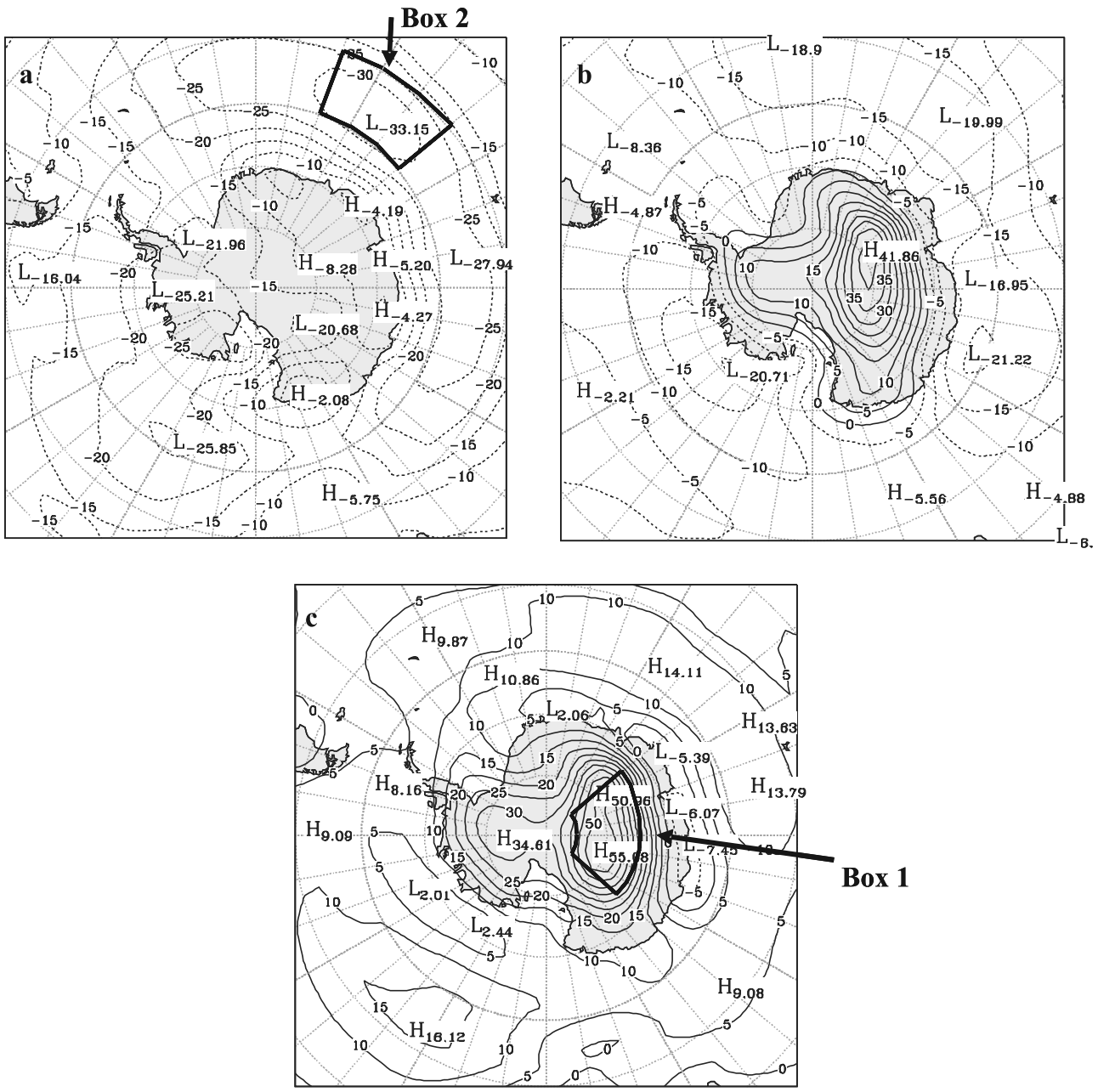

Figure 3. Annual mean 500 hPa geopotential height differences (in gpm) from 1979–2001 for (a) ERA-40 minus JRA-25, (b) ERA-40 minus NCEP1, and (c) JRA-25 minus NCEP1.

JRA-25 maintains a persistent positive difference from 1979–1995, especially compared to ERA-40, and ERA-40 shows a shift at around 1996 of ~20 gpm when it better aligns with the other reanalyses. The differences in JRA-25 are primarily related to the assimilation of the TOVS 1-D radiances over the Southern Ocean in JRA-25 (K. Onogi, personal communication, 2006). However, it is uncertain if the change in ERA-40 at 1996 is real or an artifact related to the change in the High-resolution Infrared Radiation Sounder (HIRS) assimilation in ERA-40 discussed later in section 4. Nonetheless, despite the differences between the reanalyses in these regions, Figure 4 clearly demonstrates that the interannual variability is well-captured by all reanalyses.

[16] In a reanalysis system, forecast precipitation minus evaporation/sublimation (precipitation minus evaporation (P − E)) does not necessarily equal moisture flux convergence, as the reanalysis is based on observations with systematic bias corrections (addition or removal of atmospheric moisture in the humidity analysis) that may lead to an imbalance in the atmospheric moisture budget. The tropics (30°N–30°S) in ERA-40 are a clear example of this problem, as forecast precipitation exceeds forecast evaporation from 1973–1995, related to the assimilation of satellite data to correct what is perceived to be a too-dry

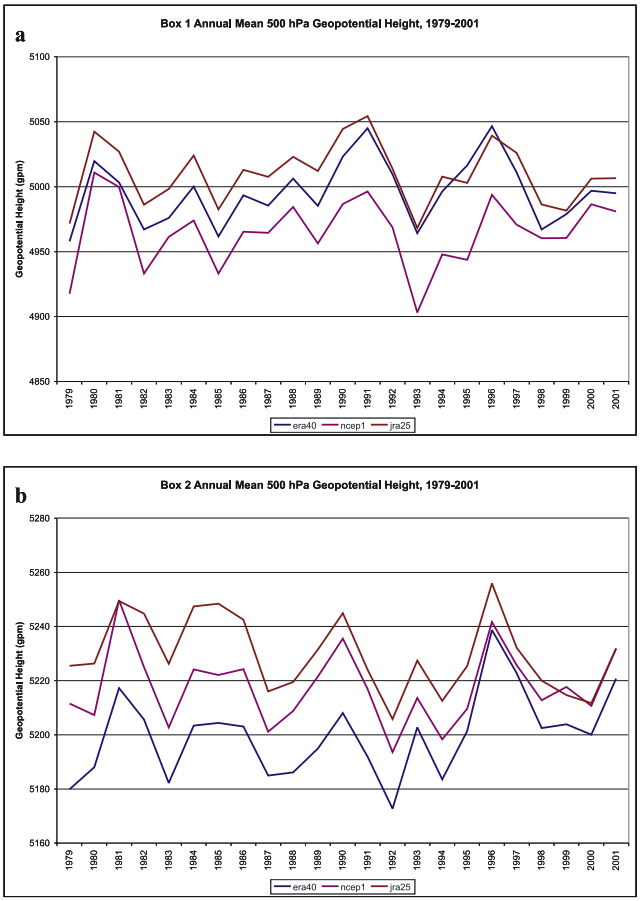

Figure 4. Annual mean 500 hPa geopotential heights averaged in (a) the Antarctic interior (75°–85°S, 50°–130°E; box 1 in Figure 3) and (b) over the Southern Ocean (50°–60°S, 20°–30°E; box 2 in Figure 3). Note different vertical scales in Figures 4a and 4b.

background state over the tropical oceans in ERA-40 [*Andersson et al.*, 2005; *Bengtsson et al.*, 2004a]. Although *Cullather et al.* [2000] demonstrate that forecast values of P − E are 27% less than those obtained from moisture flux convergence over the Arctic in ERA-15, *Bromwich et al.* [2002] demonstrate that forecast P − E and moisture flux convergence are balanced in the Arctic and Antarctic on annual timescales in ERA-40. Because of the near "hydrologic balance" of ERA-40 in the polar regions, the paper will henceforth assume that forecast P − E is accurate in the polar regions, making it a reliable approximation of snow accumulation over the Antarctic ice sheet.

[17] Nonetheless Antarctic forecast P − E in ERA-40 (Figure 5) demonstrates a jump at around 1979, when the TOVS data were first assimilated into ERA-40. This discontinuity was first presented by *van de Berg et al.* [2005] for the solid precipitation over Antarctica in ERA-40. Figure 5 shows that the changes are largest over the continental interior, particularly over the highest elevations where P − E increases of 50% occur approximately at 1979. *Bromwich and Fogt* [2004] show large changes in the MSLP and 500 hPa geopotential height patterns in terms of both their correlation (as in ERA-40) with observations and mean bias (as in NCEP1) before and after 1979. Examining the changes in ERA-40 by seasons (not shown) reveals that the largest differences in the circulation before and after 1979 across the entire Southern Ocean are found in the summer and fall. These differences are presented in Figures 6a–6b, with those differing significantly from zero at the $p < 0.05$ level shaded. Although Figures 1 and 2 show the largest differences between ERA-40 and NCEP1 compared with observations in the winter, the winter height differences (as in Figures 6a–6b) are only observed in the South Pacific, in the same region as presented by *Bromwich and Fogt* [2004, Figure 10]. In comparison, large differences in austral summer and fall are not just confined to the South Pacific, but are observed across the entire Southern Ocean (Figures 6a–6b). The pattern in Figures 6a–6b suggests an adjustment to the common wave-3 Rossby longwave pattern [e.g., *Raphael*, 2004] with an amplified ridge-trough system, especially in the South Pacific. Naturally, this adjustment leads to changes in the meridional moisture flux, particularly in the stationary eddies (not shown). The changes in the total meridional moisture flux are plotted in Figures 6c–6d, with negative differences representing more poleward transport of moisture during the 1979–2001 period. Superimposed on Figures 6c–6d are the changes in the longwave pattern from Figures 6a–6b, whose implied geostrophic circulation changes clearly explain the differences in the meridional moisture flux. In turn, the increased meridional moisture flux leads to the marked changes in precipitation (and therefore P − E or snow accumulation over the ice sheet). This is seen in Figures 6e–6f, which presents the ratio of the 1979–2001 over the 1958–1978 precipitation. The areas with more poleward moisture flux correspond to increases in the precipitation during the 1979–2001 period, whereas areas where the meridional moisture flux becomes more equatorward during the 1979–2001 period are represented by near zero changes in the total precipitation ratio. The slight increases in these regions can be explained by changes in the eddy component of the meridional moisture flux (not shown), which is more poleward everywhere across Antarctica and into the Southern Ocean.

[18] Because observations of precipitation are very limited in Antarctica, one of the best ways to understand the precipitation variability is through the reanalysis products. The period for which ERA-40 precipitation might be considered most reliable is subsequent to the discontinuity that occurred in 1979 (Figure 5). Unfortunately, the bias correction scheme did not fully adjust to the satellite data until 1985 in ERA-40 (Adrian Simmons, personal communication, 2006), rendering the ERA-40 precipitation at high southern latitudes questionable before this period [*Turner et al.*, 2005]. Therefore *Monaghan et al.* [2006] examined the variability and trends in Antarctic forecast precipitation minus evaporation (P − E) from limited area modeling fields and reanalysis from 1985 onward. Table 2 presents the 1985–2001 trends over the grounded ice sheet from NCEP2, ERA-40 and JRA-25, adapted from *Monaghan et al.* [2006]. The trend in NCEP2 is positive, while the ERA-40 and JRA-25 trends are negative. Although the trends are not statistically different from zero, their range clearly indicates that Antarctic precipitation variability is markedly different between the reanalyses. When comparing the temporal

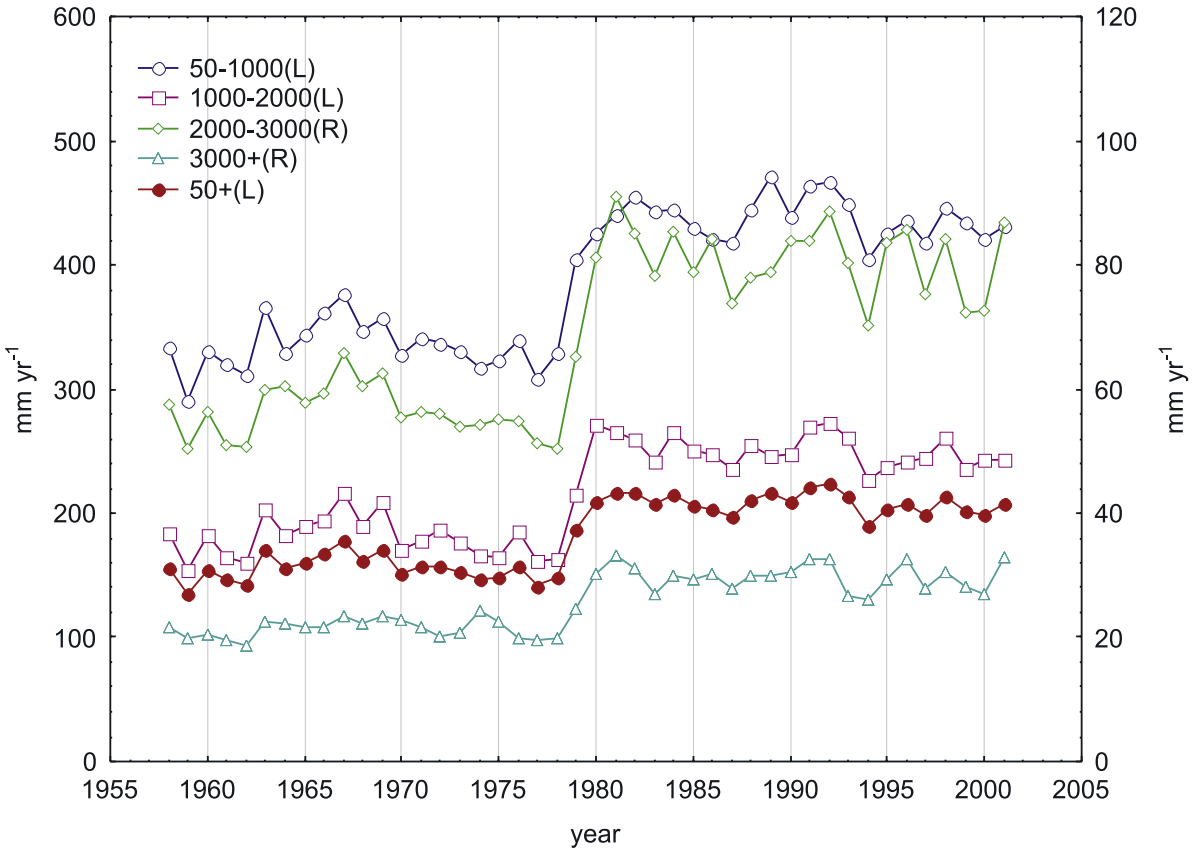

Figure 5. Annual mean area-weighted ERA-40 Antarctic forecast precipitation minus evaporation (P − E) (equals snow accumulation) for various regions based on elevation, after *van de Berg et al.* [2005]. Key defines elevation bands (in m) considered with corresponding vertical scales (left, L; right, R).

accumulation changes from the reanalyses with ice core records, *Monaghan et al.* [2006] find that ERA-40 is better aligned with the observations than NCEP2 or JRA-25. They also note that the long-term annual NCEP2 P − E is anomalously low over most of interior and coastal East Antarctica, and JRA-25 P − E is too high over the Antarctic interior, compared to observations. The latter claim is verified here in Figure 7, which displays the 1979–2004 annual mean JRA-25 precipitation (closely resembles accumulation over the interior of the continent as evaporation is negligible there [*Bromwich et al.*, 2004]) minus the climatological Antarctic accumulation estimate of *Vaughan et al.* [1999] derived from surface observations. Although Figure 7 shows large local differences mostly related to smoothed topography in JRA-25, a dominant feature is the excessive precipitation (30–60 mm) over the interior of the continent, much larger than seen in any other reanalysis [*Monaghan et al.*, 2006]. Notably, the *Vaughan et al.* [1999] study may underestimate the coastal accumulation [*van de Berg et al.*, 2006], which helps to explain some of the large differences at the edge of the continent (evaporation is also playing a role), and Onogi et al. (submitted manuscript, 2007) relate the precipitation excess over the interior to the spectral truncation (Gibbs phenomenon) of water vapor in regions where the saturation vapor pressure is small because of low air temperatures. Because of this deficiency in JRA-25 and those identified in NCEP2, *Monaghan et al.* [2006] conclude that the precipitation trend from ERA-40 is the most realistic, as ERA-40 has the best agreement with available observations from 1985–2001 over the majority of the continent.

[19] A last topic to consider for Antarctica and the Southern Hemisphere is the Southern Annular Mode (SAM). The SAM has generally been considered a zonally symmetric or annular structure with pressure anomalies of opposite sign in the middle and high latitudes [*Thompson et al.*, 2000]. This climate mode contributes a significant proportion of Southern Hemisphere climate variability (typically ~35%) from daily [*Baldwin*, 2001] to decadal timescales [*Kidson*, 1999]. When pressures are below (above) average over Antarctica the SAM is said to be in its high (low) index or positive (negative) phase. There are two common definitions of the SAM, one using differences in the standardized pressures from 40°S and 65°S [*Gong and Wang*, 1999] and the other the leading empirical orthogonal function (EOF [*Thompson et al.*, 2000]) of MSLP or geopotential height throughout the troposphere. Reanalyses are generally used to construct SAM indices due to their spatial completeness, however, the erroneous MSLP trends in the NCEP/NCAR reanal-

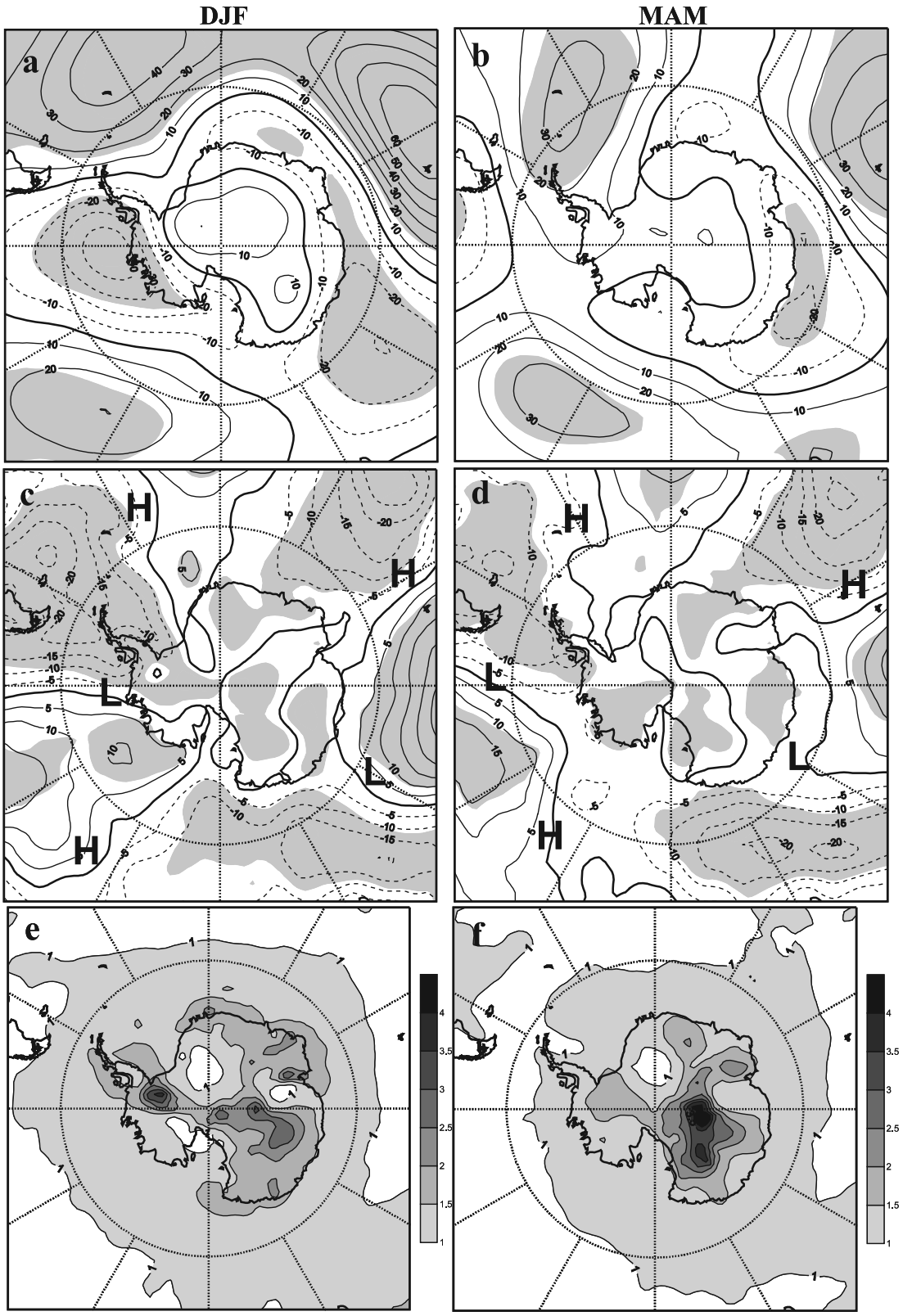

Figure 6. (a and b) ERA-40 1979–2001 minus 1958–1978 500 hPa height differences in gpm. (c and d) ERA-40 1979–2001 minus 1958–1978 total meridional moisture flux differences in kg m^{-1} s^{-1}, with the height change centers from Figures 6a–6b superimposed with H (height rises) and L (height decreases). (e and f) ratio of the 1979–2001 over the 1958–1978 precipitation (unitless). Shaded regions in Figures 6a–6d represent differences significant from zero at the $p < 0.05$ level using a two-tailed Student's *t*-test. Contour interval is 10 gpm in Figures 6a and 6b; 5 kg m^{-1} s^{-1} in Figures 6c and 6d; and 0.5 starting at 1 in Figures 6e and 6f. Zero contour is thickened in Figures 6a–6d for ease in interpretation.

Table 2. Comparison of the Reanalyses' Trends and 90% Confidence Intervals of Precipitation Minus Evaporation (P − E) Over the Grounded Antarctic Ice Sheet, 1985–2001, as by *Monaghan et al.* [2006]

Reanalysis	Trend, mm yr^{-2}
ERA-40	−0.29 ± 0.62
JRA-25	−0.47 ± 0.88
NCEP2	0.58 ± 0.74

yses (cf. Figure 2b) and the low correlation of ERA-40 MSLP and MSLP from station observations (cf. Figure 1a) compromise the reliability of long-term SAM indices derived from the reanalyses. In response, *Marshall* [2003] presents an index for the SAM (updated at http://www.nerc-bas.ac.uk/icd/gjma/sam.html) using available station observations near the 40°S and 65°S parallels employed in the *Gong and Wang* [1999] definition. Table 3 presents various SAM trends from the major reanalyses calculated over the 1979–2001 period using the *Gong and Wang* [1999] definition along with the corresponding *Marshall* [2003] values. Here, the statistical significance was determined using a Student's two-tailed *t*-test, tested against the null hypothesis that the trends are zero, with the degrees of freedom for each series reduced by the lag-1 autocorrelation; also presented are the 95% confidence intervals to provide an estimate of the uncertainty about the trend. During this period, the reanalyses are fairly consistent and show the strongest trends in the monthly, summer, and autumn data, with varying levels of statistical significance. All methods also agree that the trends are statistically insignificant and near zero during winter and spring. However, using a Varimax-rotated principal component (RPC) time series as the definition of the SAM produces more discrepancies between the various reanalyses (Table 4). Rotation of the EOFs was conducted as it simplifies the structure by reducing the number of factors onto which a variable will load strongly [*Richman*, 1986], often providing more physical meaning to these statistical SAM representations. Because the SAM may not always be the leading mode in the seasonal rotated EOFs, the RPC time series used to define the SAM here is chosen by the score time series which has the strongest correlation with the *Gong and Wang* [1999] index from Table 3. Although some of these differences in the RPC-based SAM indices are likely related to the methodology (including rotation type and number of factors retained for rotation), the trends are quite different from those presented in Table 3, especially for the ERA-40 reanalysis and all reanalyses using the monthly data. The monthly RPC time series trends are all near zero and not statistically significant in Table 4. This Table also shows that ERA-40, unlike the other two reanalyses or the *Marshall* [2003] index, does not produce a statistically significant trend during autumn or summer, but rather produces a strong and statistically significant negative trend during the winter and a weaker negative trend, still marginally statistically significant, during the spring. The lack of significant trends in summer in ERA-40 is related to the shared variability between the El Niño – Southern Oscillation (ENSO) modes and the SAM [e.g., *Fogt and Bromwich*, 2006; *L'Heureux and Thompson*, 2006], as more than one loading pattern for ERA-40 during the summer has a strong correlation with both SAM and ENSO indices (not shown). Nonetheless, Tables 3 and 4 clearly indicate that there are large differences in the SAM trends depending on the definition and reanalyses employed. These differences must be considered when using the SAM to explain other climate trends in the Antarctic.

4. Evaluations in the Arctic

[20] As noted in section 1, the differences between the reanalyses and observations in the Antarctic are much larger than those observed in the Arctic, primarily due to the larger observational data density in the Arctic region. *Serreze et al.* [2007] further show that ERA-40 and NCEP1 have comparable magnitudes of the vertically integrated mass-corrected atmospheric energy fluxes across 70°N (Figure 8), the latitude with the greatest spatial density of radiosondes globally. The thermal (sensible heat) meridional flux is similar in both reanalyses. The latent heat fluxes are also very similar, except that NCEP1 tends to yield slightly higher summer peaks as well as slightly higher winter minima. *Cullather et al.* [2000] demonstrate that NCEP1 and ERA-15 display comparable magnitudes of the moisture flux convergence derived from the radiosonde network around 70°N, thereby showing that not only do these two reanalyses agree with each other in the latent heat flux across 70°N, but they also have good agreement with observations. There is less agreement in the meridional geopotential energy flux which may be related to the higher vertical resolution of ERA-40 in the upper troposphere and lower stratosphere, where geopotential is large, although *Serreze et al.* [2007] also suggest these values may be incorrectly calculated at ECMWF. ERA-40 also shows

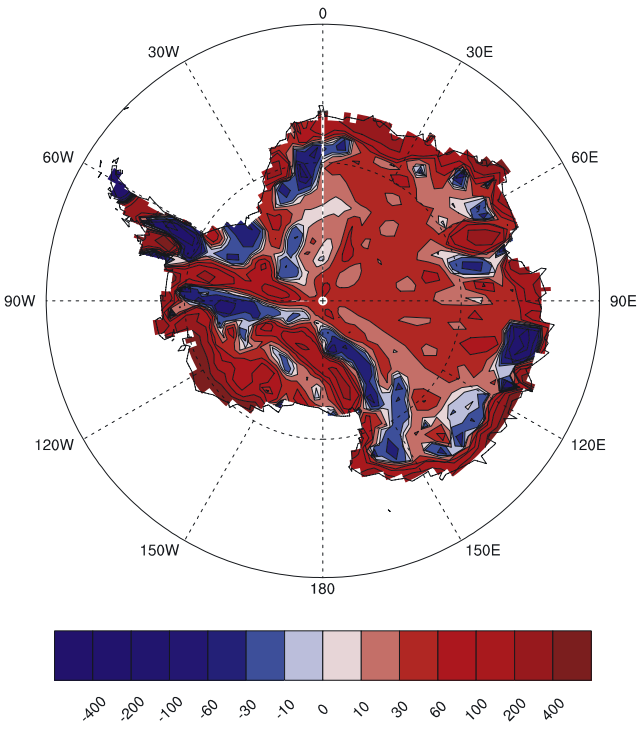

Figure 7. JRA-25 1979–2004 annual mean precipitation minus the long-term average accumulation estimate of *Vaughan et al.* [1999] based on surface observations in mm.

Table 3. Comparison of the Trends (Per Decade) Over 1979–2001 and the 95% Confidence Intervals in the *Gong and Wang* [1999] Derived SAM Indices for Different Reanalyses[a]

SAM Indices [*Gong and Wang*, 1999]	ERA-40	NCEP2	JRA-25	*Marshall* [2003]
Monthly	0.34 ± 0.17***	0.39 ± 0.17***	0.26 ± 0.18***	0.23 ± 0.23*
Summer	0.87 ± 0.64**	0.85 ± 0.65**	0.73 ± 0.66**	0.78 ± 0.48***
Autumn	0.64 ± 0.63**	0.72 ± 0.61**	0.59 ± 0.63*	0.61 ± 0.37***
Winter	0.10 ± 0.67	0.22 ± 0.67	0.07 ± 0.73	−0.16 ± 0.59
Spring	0.32 ± 0.63	0.41 ± 0.62	0.08 ± 0.70	0.17 ± 0.51

[a]Also presented are the trends in the *Marshall* [2003] index. One asterisk, two asterisks, and three asterisks indicate trends significant at $p < 0.1$, <0.05, and <0.01 levels, respectively.

some evidence of a slight downward trend in the meridional geopotential flux. Differences in the moist static energy flux (sum of sensible, latent, and geopotential fluxes) hence primarily result from differences in the geopotential flux. For the annual average, ERA-40 and NCEP1 yield a total moist energy flux across 70°N (weighed by the area of the polar cap) of 101 W m^{-2} and 103 W m^{-2}, respectively. Although no such comparisons have been conducted in the Antarctic, it is expected that the differences in Figure 8 for the Arctic are smaller than those in the Antarctic.

[21] *Bromwich and Wang* [2005] find good agreement between NCEP1 and ERA-40 and two independent rawinsonde archives from the edge of the Arctic Ocean; they along with *Bromwich et al.* [2002] do note a lower-to-middle tropospheric cold bias in ERA-40 over the central Arctic Ocean, with ERA-40 exhibiting lower geopotential heights. Figure 9a shows that the annual average 500 hPa geopotential height difference between ERA-40 and NCEP1 over the central Arctic Ocean in 1996 is as large as 20 gpm; however, from 1997 onward the differences are near zero (Figure 9b). According to ECMWF, the ERA-40 cold bias is related to the assimilation of the HIRS data in ERA-40. In 1997, changes to the thinning, channel selection, and quality control of the HIRS data were applied in attempts to reduce ERA-40's tropical precipitation bias [*Bengtsson et al.*, 2004a; *Andersson et al.*, 2005]. Notably, these changes also removed the Arctic Ocean cold bias in ERA-40. Although the differences in Figure 9 are small compared to those seen in the Antarctic (cf. Figures 3, 4, and 6), it is important to be informed that these changes are artifacts in ERA-40 as compared against available observations and the other contemporary reanalyses. The smaller differences in the Arctic compared to the Antarctic again demonstrate the higher level of reanalysis skill in the Northern Hemisphere high latitudes.

[22] However, there are some substantial differences in the Arctic region worth mentioning. *Serreze et al.* [2005] compared the precipitation biases in ERA-40, NCEP1 and the Global Precipitation Climatology Project version-2 (GPCP) of *Adler et al.* [2003] from 1979–1993 against gridded fields based on station precipitation gauge measurements that include adjustments for gauge undercatch of solid precipitation (Figure 10). The biases reveal that NCEP1 produces excessive precipitation during the height of summer over the Arctic land masses, while the biases of ERA-40 and the GPCP are smaller and very similar to each other. *Serreze et al.* [2003] and *Serreze and Hurst* [2000] relate the large positive summer precipitation bias in NCEP1 to excessive convective precipitation and high evaporation rates. *Serreze et al.* [1998] also demonstrate that there is excessive downwelling solar radiation in NCEP1 during June, which enhances the evaporation and convective activity in NCEP1. Evaluation of the NCEP2 reanalysis shows no improvement in these respects. Within the major Arctic watersheds (the Ob, Yenisei, Lena, and Mackenzie), ERA-40 captures from 60 to 90% of the observed temporal precipitation variance, which is much higher than that captured by NCEP1 and GPCP. A study by *Déry and Wood* [2004] similarly finds good agreement between ERA-40 and observed precipitation estimates within the Hudson Bay Basin, while *Su et al.* [2006] also find good agreement between ERA-40 precipitation and observations across all of the Arctic river basins. ERA-40 estimates of net precipitation (P − E) from the aerological budget (adjusting the vapor flux convergence by the tendency in precipitable water) and from the forecasts of P and E also tend to be more closely in balance than corresponding estimates from NCEP1 and ERA-15 [*Serreze et al.*, 2006].

[23] To better understand the differences between the radiation terms in the reanalyses as given by *Serreze et al.* [1998], it is necessary to examine how each reanalysis simulates polar clouds and the radiative impacts of these clouds. In Barrow, Alaska (71°N, 156°W), an Atmospheric Radiation Measurement (ARM) suite of instruments has routinely measured (since 1998) cloud cover and both shortwave and longwave radiation, among many other

Table 4. As in Table 3, but for Varimax Rotated Principal Component-Based SAM Indices[a]

SAM RPC Indices	ERA-40	NCEP2	JRA-25	*Marshall* [2003]
Monthly	−0.01 ± 0.18	0.09 ± 0.18	0.10 ± 0.19	0.23 ± 0.23*
Summer	0.30 ± 0.72	0.79 ± 0.65**	0.91 ± 0.62***	0.78 ± 0.48***
Autumn	0.21 ± 0.66	0.61 ± 0.62*	0.59 ± 0.62*	0.61 ± 0.37***
Winter	−0.81 ± 0.58**	−0.48 ± 0.65	−0.42 ± 0.70	−0.16 ± 0.59
Spring	−0.57 ± 0.64*	−0.64 ± 0.63**	−0.43 ± 0.70	0.17 ± 0.51

[a]Also presented are the trends from *Marshall* [2003] for comparison. One asterisk, two asterisks, and three asterisks indicate trends significant at $p < 0.1$, <0.05, and <0.01 levels, respectively.

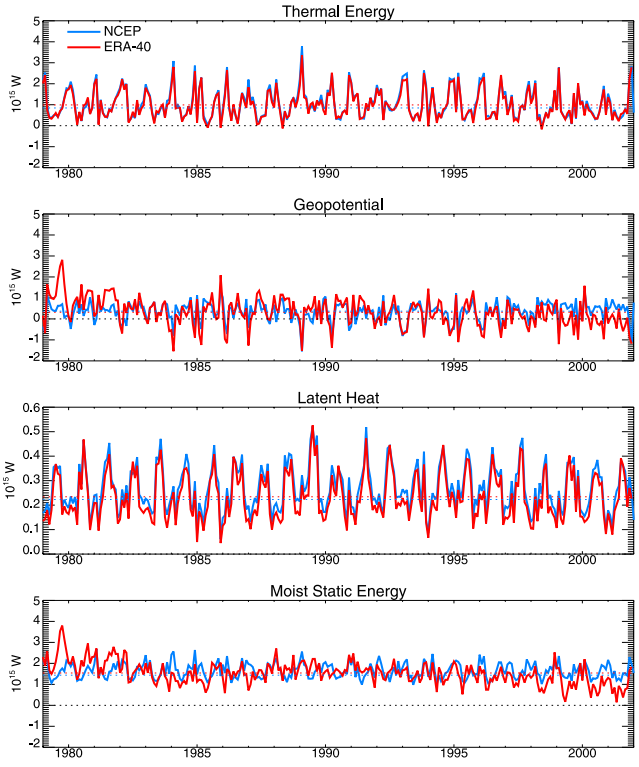

Figure 8. Monthly mean energy components across 70°N from ERA-40 (red) and NCEP1 (blue) for 1979–2002. From *Serreze et al.* [2007].

variables (see online at http://www.arm.gov/sites/site_inst.php?loc = nsa&facility = C1). We have compared the cloud fraction and downwelling shortwave radiation measurements with output from ERA-40, NCEP1, and JRA-25. The results are shown in Figure 11 for a summer month, June 2001. Figure 11a shows that the cloud fraction is well-captured by ERA-40, indicating that ERA-40 does a good job of simulating overall cloud cover and its variability. The correlation between the two time series in Figure 11 is 0.49. However, the downwelling shortwave radiation during the solar maximum is overpredicted considerably (by up to ~300 Wm^{-2} in extreme instances), especially during periods of overcast or cloudy conditions. For NCEP1, a similar overprediction of the downwelling shortwave radiation of ~300 Wm^{-2} is seen (Figure 11b). However, it is apparent that NCEP1 does not capture the cloud variability (the simulated and observed cloud fractions are correlated at only 0.08), so this bias is related to deficient cloud cover in NCEP1. JRA-25 ranks between ERA-40 and NCEP1 in its simulation of the variations of cloudiness in June (Figure 11c); the mean cloud fraction is approximately midway between that of ERA-40 and NCEP1, and the correlation between the JRA-25 and ARM cloud fractions is 0.32. During periods when the NCEP1 and JRA-25 cloud fractions are aligned with the observed cloud fractions (i.e., 2 and 15 June for NCEP1; 2 and 17 June for JRA-25), the downwelling shortwave radiation is also in agreement with the measured values.

[24] Given the differences in cloudiness simulated by the three reanalyses, it is not surprising that ERA-40 does a much better job of capturing the variations in the longwave radiation, with the differences of ~50 Wm^{-2} occurring only when there are differences between the reanalysis and observed cloud fraction (Figure 12a). The discrepancies between NCEP1, JRA-25, and observed cloud cover are also associated with large errors (~75 Wm^{-2}) in the downwelling longwave radiation component (Figure 12b and 12c).

[25] The fact that ERA-40 reproduces much of the cloud variability and associated fluctuations of the downwelling longwave radiation, but overpredicts the downwelling shortwave radiation, suggests there are problems in the way that ERA-40 handles the transmission of shortwave radiation

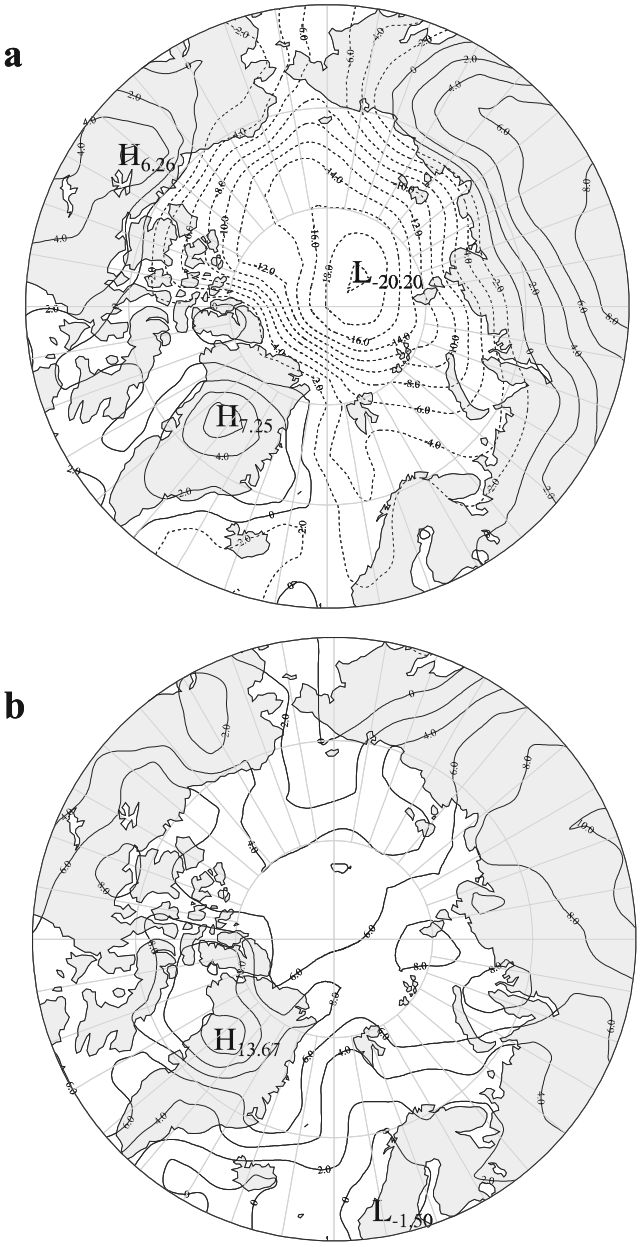

Figure 9. Annual mean ERA-40 minus NCEP1 500 hPa geopotential height difference (in gpm) for (a) 1996, before the High-resolution Infrared Radiation Sounder (HIRS) assimilation change and (b) 1997, after the HIRS assimilation change. Adapted from *Bromwich and Wang* [2005].

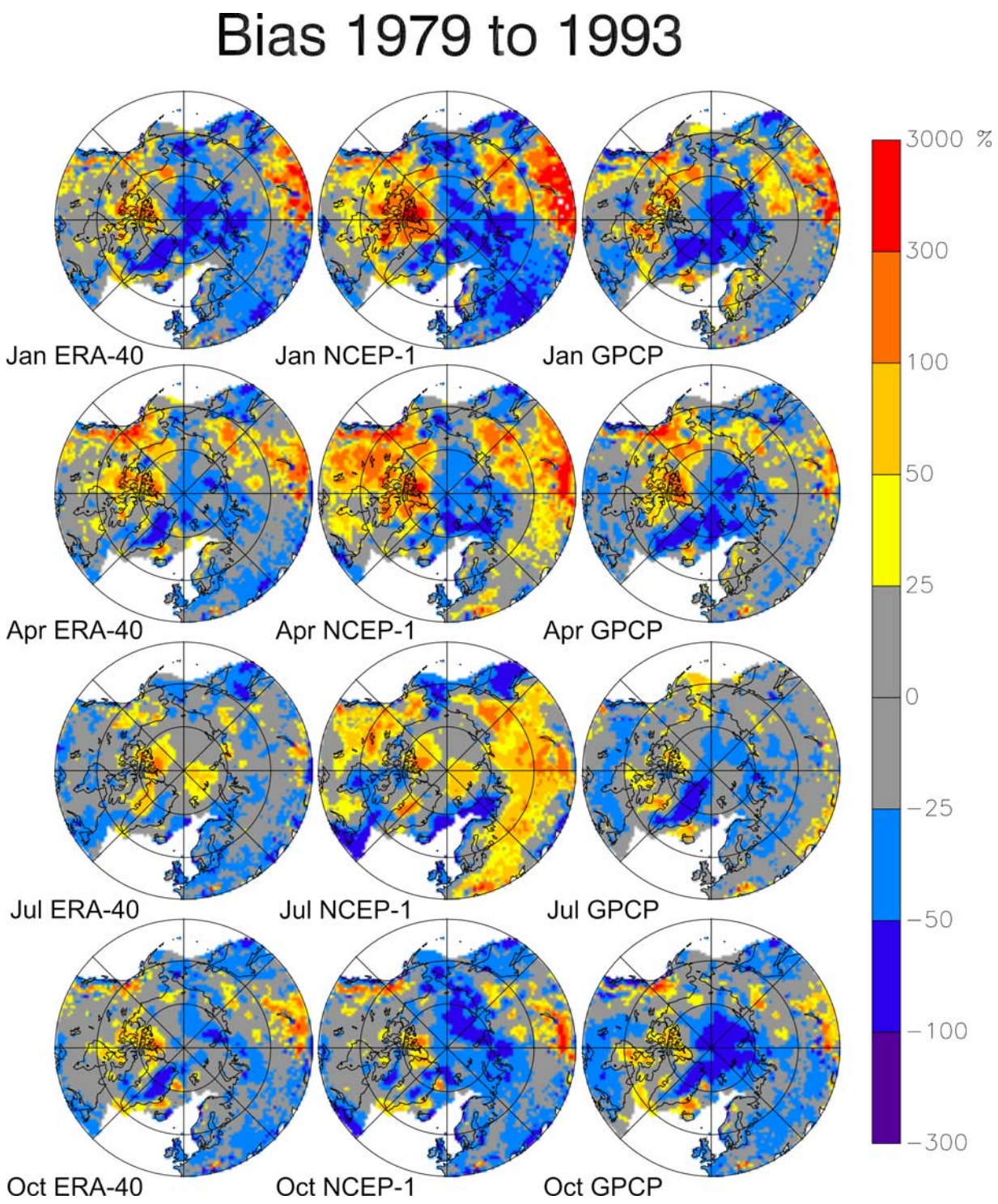

Figure 10. Mean bias (1979–1993) of accumulated precipitation (in %) compared against a corrected gridded archive of station observations for January (first row), April (second row), July (third row), and October (last row) for ERA-40, NCEP1, and GPCP, from *Serreze et al.* [2005].

through the clouds. Meanwhile, Figures 11–12 indicate that NCEP1 and JRA-25, although not skillful in simulating the cloud variability/cover, do capture the primary impacts of clouds on the radiation budget, especially in the downwelling shortwave radiation component. To examine this disparity further, we have compared the mean cloud radiative forcing (CRF) in the different reanalyses. The CRF is defined here as the area-weighted difference between the net surface radiation (in W m^{-2}) with cloud fraction F and the corresponding clear-sky net surface radiation from 70°–90°N. Note that this definition extends the conventional definition of cloud radiative forcing, which is integrated over the observed (or simulated) distribution of cloud fractions. The CRF, evaluated from ERA-40, NCEP1 and

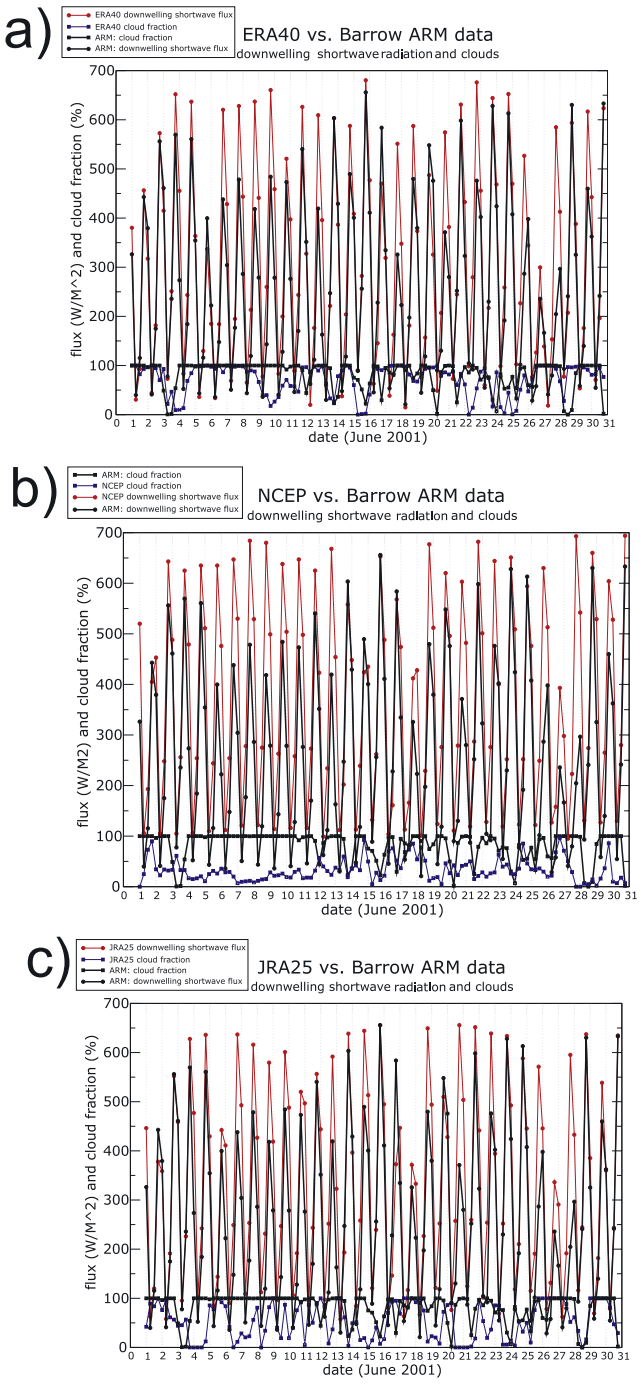

Figure 11. Observed downwelling shortwave radiation (top) and cloud fraction (bottom) data for Barrow Atmospheric Radiation Measurement (ARM) site during June 2001 compared with equivalent data from (a) ERA-40, (b) NCEP1, and (c) JRA-25.

JRA-25 as a function of cloud fraction and calendar month is presented in Figure 13. Large differences are immediately apparent between the reanalyses, indicating that the impacts of clouds on the net surface radiation are substantially different in the three reanalyses. ERA-40 (Figure 13a) has a very sharp gradient in the cloud radiative forcing for large cloud fractions. Thus even cloud fractions as high as 0.85 do not have a strong impact on the radiation. NCEP1 (Figure 13b), however, produces a much smoother distribution of the cloud radiative forcing, spreading the impact on the radiation to much lower cloud fraction values. The CRF resulting from 80–100% cloud cover exceeds 50 W m^{-2} during the cold season (October–March) in NCEP1. JRA-25, on the other hand, shows much weaker CRF (20–30 W m^{-2}) under overcast conditions in both winter and summer (Figure 13c). The JRA forcing by clouds shows a weaker dependence on cloud fraction than ERA-40

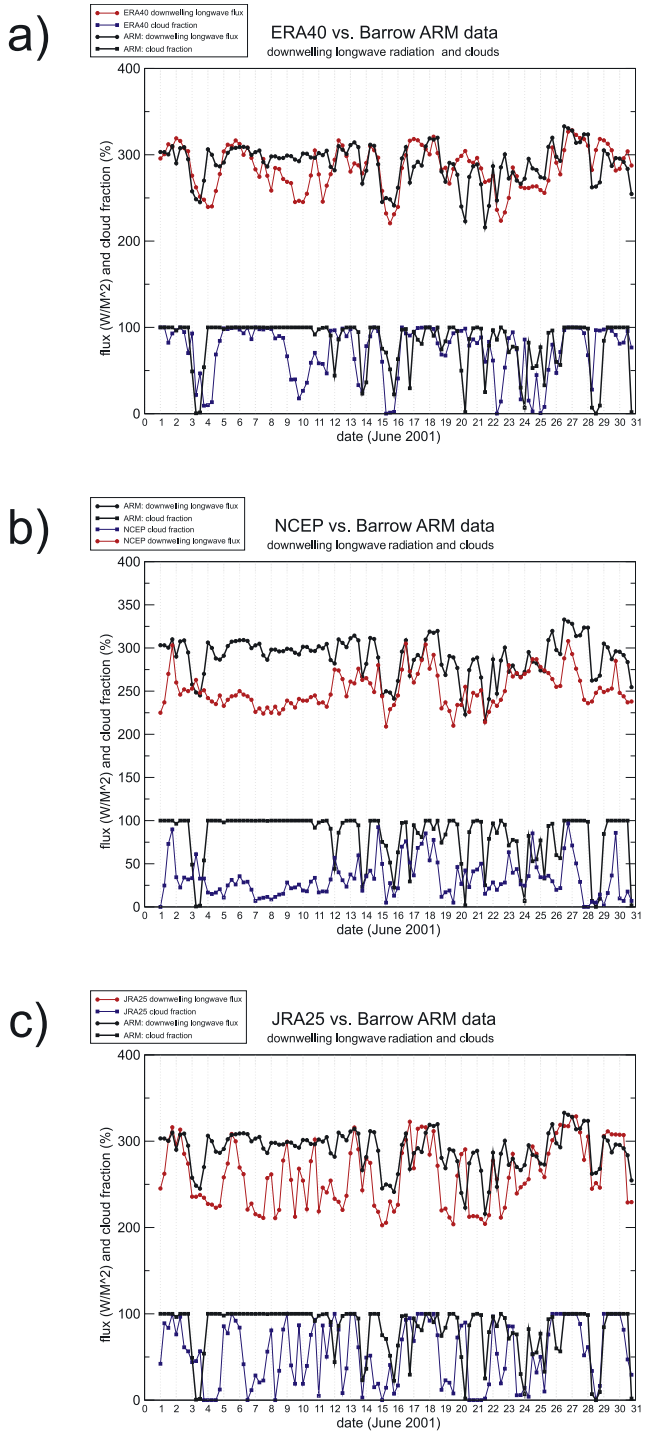

Figure 12. As in Figure 11, but for downwelling longwave radiation.

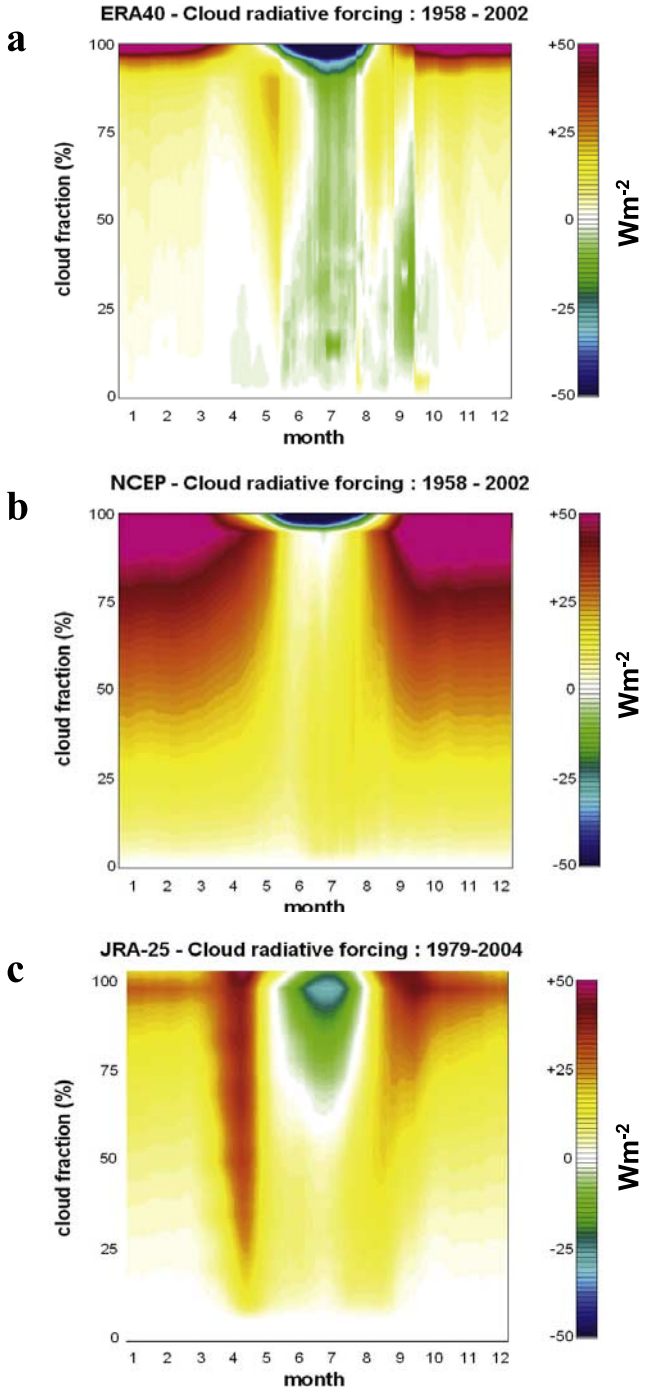

Figure 13. Annual cycle of mean cloud radiative forcing (1958–2002) by cloud fraction for (a) ERA-40, (b) NCEP1, and (c) JRA-25 for 1979–2004. See text for details.

and NCEP1; the spring and autumn maxima in JRA-25's positive values of CRF are inconsistent with the other reanalyses and with CRF for the central Arctic on the basis of measurements at the Russian drifting ice stations [*Walsh and Chapman*, 1998, Figure 11]. When compared with the CRF derived from the Russian ice station data, NCEP1 shows the best agreement in winter and ERA-40 in summer.

[26] In summary, the radiative impacts of the clouds in the central Arctic vary widely among the three global reanalyses. All three reanalyses indicate that the CRF under overcast skies is positive in winter and negative during summer, but the magnitudes of the CRF for a particular month and cloud fraction can vary by as much as 50 W m^{-2} among the reanalyses (compared to direct radiative effect of CO_2 doubling, which is ~5 W m^{-2}). The clouds of ERA-40 and JRA-25 are too optically thin, and do not have strong enough impact on the radiation, except when the cloud fraction is very large. The simulated cloud fractions, however, are in better agreement with observations in ERA-40 and in JRA-25. Although a cloud radiation study for the Antarctic has not been published to the authors' knowledge, it is expected that a similarly deficient cloud radiative forcing in ERA-40 and JRA-25 and deficient cloud cover in NCEP1 also exist in the high southern latitudes.

5. Differences in the Cyclonic Behavior in Both Hemispheres

[27] The reanalyses provide powerful data for exploring cyclone activity, due to their easy access, their continuous, consistent assimilation system, and the availability of many variables (e.g., relative vorticity) that are important for cyclogenesis and cyclolysis studies. Using the cyclone tracking algorithm employed by *Hoskins and Hodges* [2002, 2005] to extend the analysis of *Hodges et al.* [2003, 2004] by considering ERA-40, JRA-25 and NCEP1 for their full periods, comparisons of the distributions for cyclone maximum intensity in the Northern and Summer Hemisphere (NH and SH, respectively) winters (DJF and JJA, respectively) are conducted for the period before and during the modern satellite era, 1958–1978 versus 1979–2001. These results are presented in Figure 14 on the basis of the 850hPa relative vorticity field, and are similar to the findings presented by *Wang et al.* [2006]. However, there are notable differences in methodology between the results presented here and those presented by *Wang et al.* [2006], namely:

[28] 1. The current study uses the cyclone tracking algorithm of *Hoskins and Hodges* [2002, 2005] while the latter uses that of *Serreze* [1995] and *Serreze et al.* [1997]. Notably, the tracking algorithm employed here is based on 850 hPa relative vorticity, while the tracking performed by *Wang et al.* [2006] uses MSLP. The latter is particularly sensitive to the large-scale background conditions (such as semipermanent pressure systems). To reduce this sensitivity, *Wang et al.* [2006] use the local Laplacian of MSLP as the measure of cyclone intensity.

[29] 2. The current analysis includes JRA-25, which was not discussed by *Wang et al.* [2006].

[30] 3. Contrary to the claim by *Wang et al.* [2006], the analysis presented here and revised by *Hodges et al.* [2004] also use a 2.0° maximum separation distance to identify matching cyclones between the various reanalyses.

[31] Figure 14 clearly shows that the reanalyses are in fairly good agreement for the maximum intensity distributions regardless of the time period considered in the NH. However, there is less agreement in the SH (Figure 14c), because of the problems seen in the reanalyses prior to the modern satellite era (Figures 1–2).

[32] To make a system-by-system comparison, the maximum intensity (in 850 hPa relative vorticity, units 10^{-5} s^{-1})

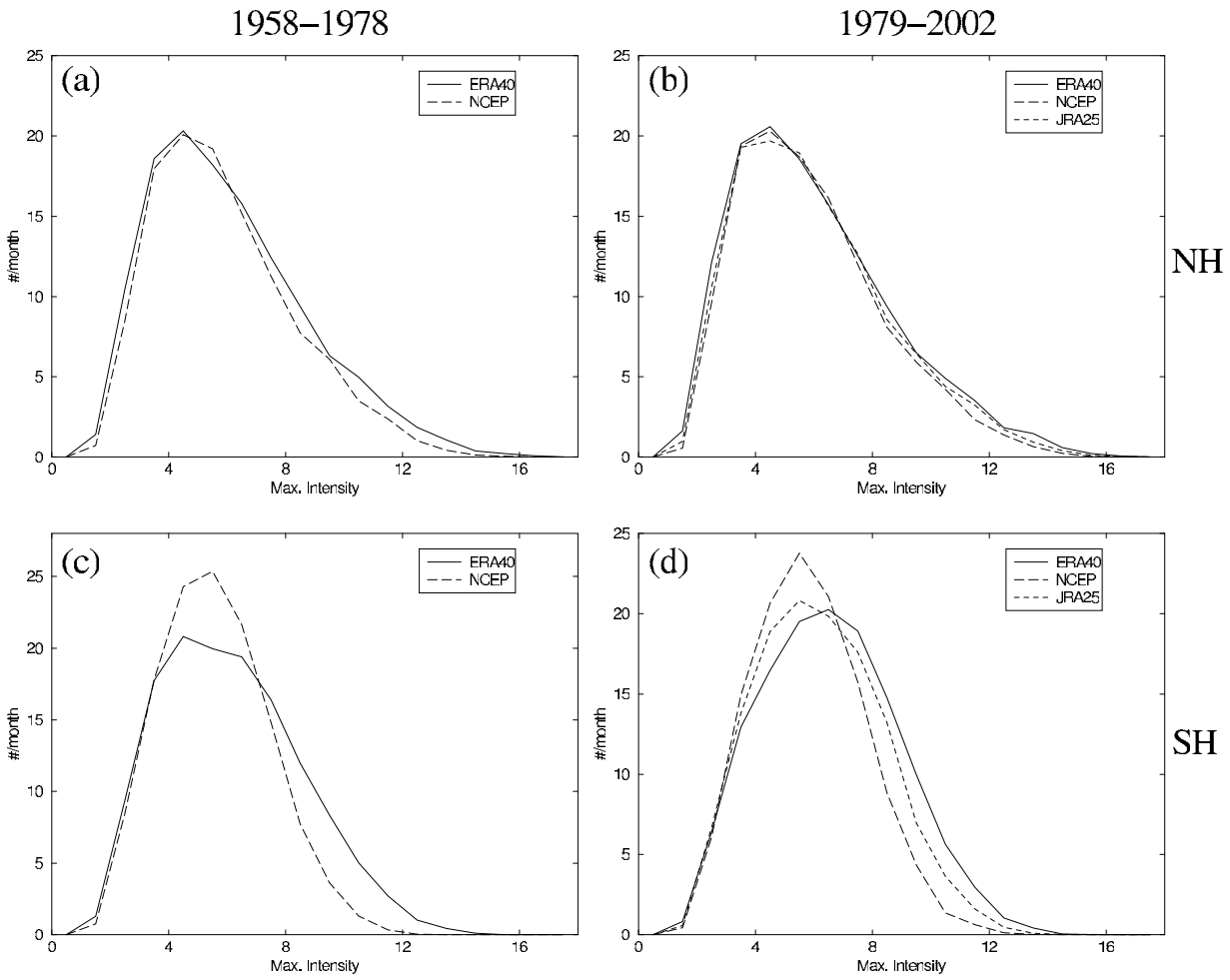

Figure 14. Mean DJF cyclone maximum intensity (in 10^{-5} s^{-1}) for the Northern Hemisphere (NH) (a–b) and Southern Hemisphere (SH) (c–d). The left column is for the 1958–1978 period, while the right column is for the 1979–2002 period. Results are extensions from *Hoskins and Hodges* [2002, 2005] and *Hodges et al.* [2003, 2004].

for matched (cases where the identical system is identified in both reanalyses; see *Bengtsson et al.* [2004b] for details) and unmatched cyclones for winter are plotted for the period before and during the modern satellite era for both the NH (DJF, Figures 15a–15b) and the SH (JJA, Figures 15c–15d) for ERA-40 and NCEP1. In the NH there is a good correspondence between systems of moderate to high intensity with only a modest improvement going into the modern satellite era. Notably, the intensity of the unmatched systems is at the weak end of the distribution, suggesting that these are likely to be small cyclones that differ between the reanalyses because of differences in the data assimilation and models. In the SH, very few systems are matched between ERA-40 and NCEP1 during the winter season for the presatellite period, when the errors of the two reanalyses are the largest (Figures 1–2). Moving to the modern satellite era, the number of matches improves dramatically, but there are still as many unmatched systems as matched ones. The unmatched systems have a broader distribution than in the NH, although it is still the more intense systems that match best. Additionally, the intensity even of matched systems is more different between the two reanalyses in the SH than in the NH, even during the modern satellite era, reflecting the differences seen in Figure 14. This suggests that storm tracking in the SH is highly dependent on the reanalysis employed, which is not surprising given that the reanalyses produce quite different trends of the SAM (which monitors the strength of the meridional pressure gradient in the SH) during austral winter (Tables 3 and 4). Similar findings for the modern satellite era are obtained when matching is performed between ERA-40 and JRA-25 (not shown), though JRA-25 is more comparable to ERA-40 than NCEP1, reflecting the greater similarities between the ERA-40 and JRA-25 systems in terms of data assimilation and model resolution. In particular the number of matches in the SH after 1979 is significantly better than for NCEP1, probably reflecting the similarity in the methods used to assimilate the satellite radiances (Table 1).

[33] The above findings are in full agreement with the matched cyclones presented for the 1958–1977 versus 1982–2001 periods given by *Wang et al.* [2006], despite the different tracking algorithms employed. However, *Wang et al.* [2006] further examine the matches in specific regions rather than poleward of 30° latitude as is presented in Figures 14–15. Specifically related to the polar latitudes, they find in the NH excellent agreement between ERA-40

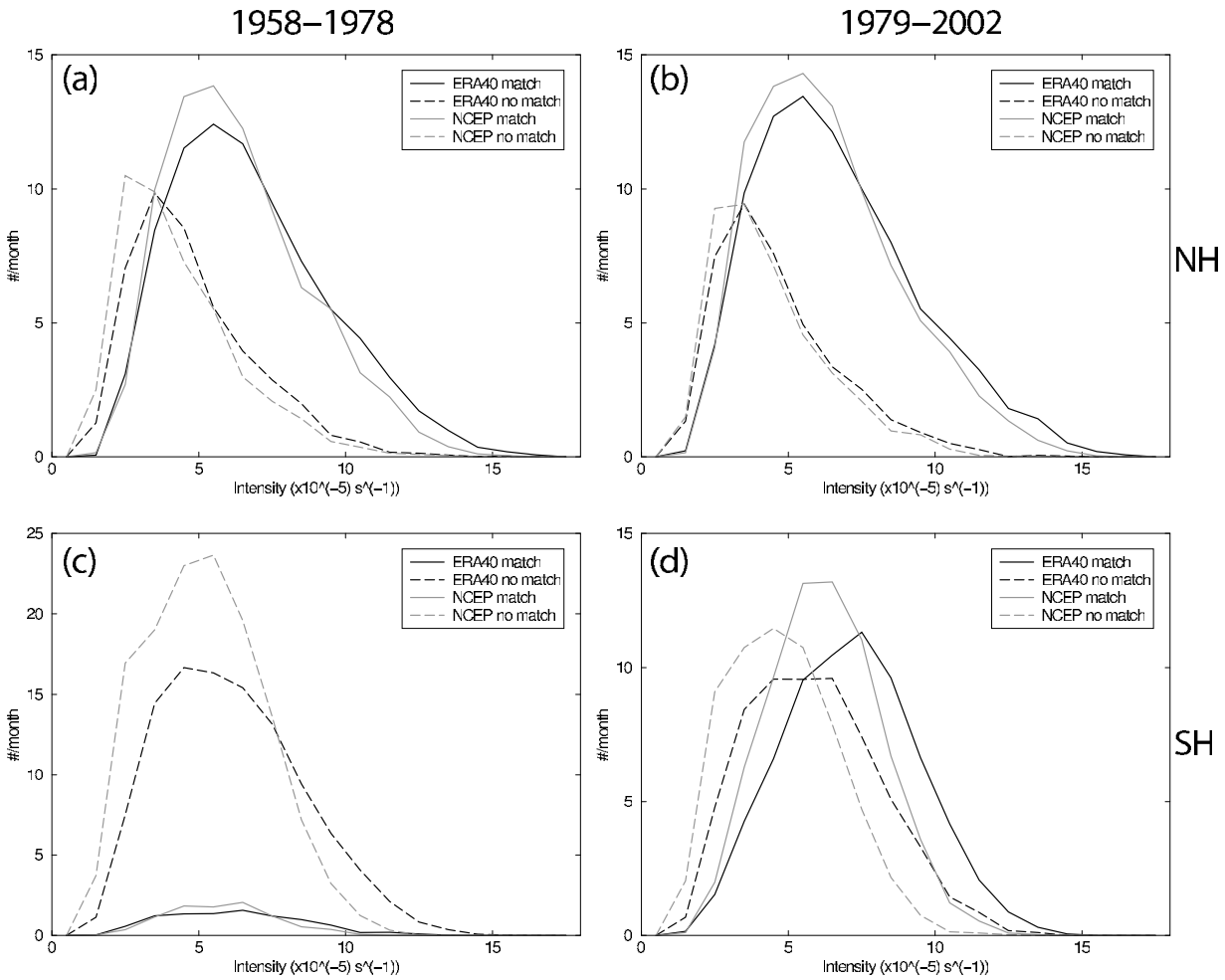

Figure 15. Mean winter cyclone intensity (in 10^{-5} s^{-1}) for 1958–1978 (a and c) and 1979–2002 (b and d) based on the number of matched systems between the reanalyses. Plots for the NH DJF are in Figures 15a and 15b; plots for the SH JJA are in the Figures 15c and 15d.

and NCEP1 in the high-latitude North Atlantic and in Northern Europe (cf. Wang et al.'s Figure 2a for these specific locations and Figures 5a–5b for comparisons). In the SH south of 60°S, broadly representing the circumpolar trough, they actually find better agreement between the reanalyses prior to 1979 than during the modern satellite era in all seasons (Wang et al.'s Figures 8a–8d). However, the comparison by *Wang et al.* [2006] is not conducted by matching between the reanalyses but simply in terms of cyclone counts in the individual reanalyses. As presented in Figure 15, there are very few cyclone matches between the reanalyses in the presatellite era, but many more in the modern satellite era. Thus the correspondence presented by *Wang et al.* [2006] in the circumpolar trough prior to 1979 may be fortuitous. The fact that the modern satellite era appears less skillful could be due to the different means of assimilating satellite observations (radiances in ERA-40 versus retrievals in NCEP1, Table 1) or due to the incorrect assimilation of PAOBS in NCEP1, for which the latter does not as strongly influence the tracking results presented here using 850 hPa relative vorticity. Therefore the exact reason for the larger differences between ERA-40 and NCEP1 during the modern satellite era south of 60°S given by *Wang et al.* [2006] is not precisely known and very surprising, given the poor winter skill of the reanalyses in Antarctica prior to 1979 (Figures1a–1b and 2a–2b). This requires further study with a different field such as vorticity as well as observing systems studies as discussed next.

[34] The cyclone tracking can also be used to explore cyclone activity in observing system experiments where various components of the observational network are removed and the analyses regenerated with the reduced observations. *Bengtsson et al.* [2004b] conducted observing system experiments to determine the differences in the ERA-40 reanalysis' ability to capture cyclones from those tracked using the full observational network minus humidity observations (control run) compared to various observational networks (Figure 16) during the DJF 1990–1991 period. In the NH, the greatest number of matches with the control, and the best alignment of system maximum intensity, occurs for the terrestrial (surface and radiosonde observations; Figure 16a) and satellite (all space-based instruments and surface pressure, Figure 16b) observing systems. Though the terrestrial system is marginally better than the satellite in terms of the number of matches, the surface network (representing surface network for the

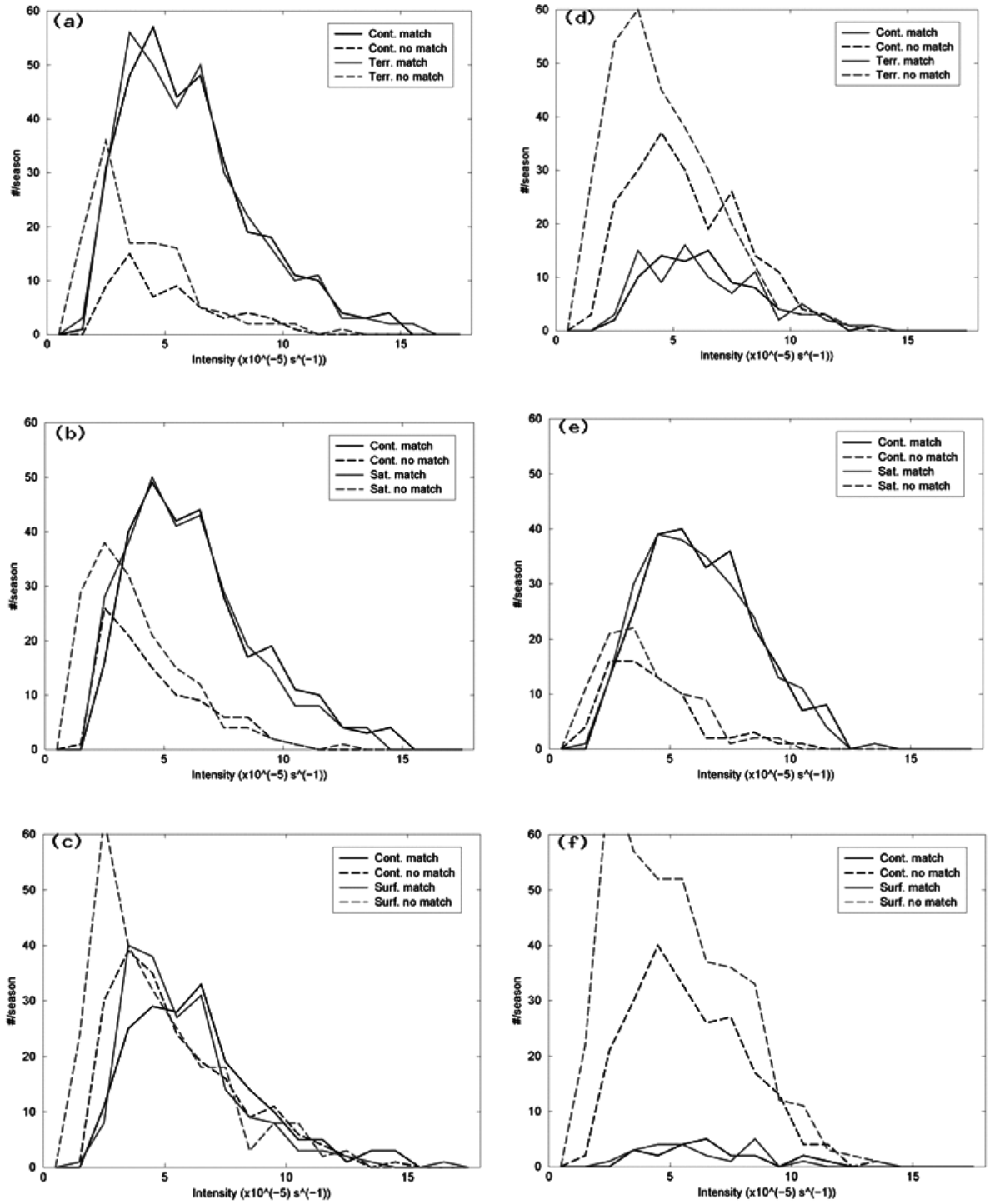

Figure 16. As in Figure 15, but for various observation system sensitivity experiments as indicated, compared against the control run of all observations (cont.) from 1990–1991 DJF. Terrestrial = surface and radiosonde observing network typical during the 1950–1979, Satellite = all space-based instruments, as well as surface pressure; Surface = only surface measurements, representative of the first half of the twentieth century. (a–c) NH and (d–f) SH. Results are extensions from work presented by *Bengtsson et al.* [2004b].

first half of the twentieth century; Figure 16c) shows only modest skill in producing matches between the two reanalyses. In the SH, the surface network (Figure 16f) provides essentially no additional information, with very few matches using this observing system. The terrestrial network (Figure 16d) provides modest skill in the number of matches and the maximum intensity, but shows a lower level of skill than seen in the surface network in the NH (Figure 16c). Clearly, the SH is dependent on satellite data (Figure 16e) to guide the reanalyses products, as this provides the greatest number of matches and best alignment in the intensity, though it is difficult to contrast with the NH as the period covers the SH summer and not the winter. The strong dependence of the reanalyses on satellite data in the SH and less dependence in the NH is in agreement with the results presented by *Sturaro* [2003].

[35] Overall, the ability for the reanalyses to track cyclones is better for the larger-scale, strong systems. In the NH, there is strong agreement even throughout the full reanalysis period, both for the cyclone intensity distribution and direct reanalysis-to-reanalysis matching. In the SH, there is much greater uncertainty in the reanalyses' ability to track cyclones during the 1979–2001 period. This is probably associated with the inability of the current satellite observing system to constrain the whole of the troposphere well in the SH because of the low spatial density of surface constraints such as surface pressure observations. Prior to this period there is essentially little correspondence between reanalyses in the SH. Observing system sensitivity experiments highlight the importance of the terrestrial observing network in the NH and the strong dependence of the reanalyses products on satellite data in the SH. These experiments will be repeated with the new ECMWF interim global reanalysis to explore, in particular, the impact of the new satellite observing systems in combination with the 4D variational data assimilation system.

6. Summary and Conclusions

[36] This paper has presented a wide array of recent knowledge regarding the status of the major global reanalyses in the polar regions, all stemming from the SCAR workshop on high-latitude reanalyses at Cambridge, UK. In the Antarctic, the reanalyses are not reliable in the non-summer months prior to the modern satellite era, and it is uncertain how reliable they are in the data sparse regions during summer [*Tennant*, 2004]. After 1979, large differences still exist between the reanalyses in the circulation, precipitation and SAM trends. It is even more apparent from this body of evidence that the reanalyses in the high southern latitudes are strongly dependent upon the satellite sounder data for guidance. The change into the modern satellite era at 1979, when vast new quantities of data were assimilated for the first time, created a sudden adjustment in the Southern Ocean and Antarctica particularly in the ERA-40 reanalysis that led to other changes in circulation-dependent variables such as precipitation.

[37] Over the central Arctic Ocean, there is a cold bias in ERA-40 related to the assimilation of the HIRS data. While there is good agreement between the reanalyses on various fluxes across 70°N, NCEP1 produces excessive summer precipitation over the Arctic landmasses. The ability of the reanalyses to predict changes in Arctic cloud cover and associated radiation (both longwave and shortwave) changes were also assessed, and it was found that NCEP1 and JRA-25 have deficient cloud cover in the Arctic. While ERA-40 does the best job of capturing the cloud variability, it produces clouds that are too optically thin (similar findings are observed in JRA-25) and thus the modeled clouds do not impact the downwelling radiation strongly enough.

[38] Storm tracking using the algorithm employed by *Hoskins and Hodges* [2002, 2005] further detailed that there is considerable skill at tracking systems for the full reanalyses time period in the NH. In the SH, there is much more uncertainty, with essentially no skill prior to 1979 indicated by the lack of similarity between the tracks and system intensity of ERA-40 and NCEP1. Care thus must be exercised when comparing results between the major reanalyses in this data sparse region of the Southern Hemisphere.

[39] It is important to note that although this synthesis has focused on the current understanding of deficiencies in the reanalyses products in the polar regions, these deficiencies do not overwhelm the fact that the reanalyses are invaluable tools for climate research. In the Antarctic, *Bromwich and Fogt* [2004] demonstrated the unprecedented skill of ERA-40 during the modern satellite era in all seasons as it produced correlations near unity and biases within measurement error for many of the conventional variables. NCEP1 also produces good correlations with observations, although winter biases remain high through the mid-1990s as NCEP1 responds to changes in the surface observation density. During the summer months, both ERA-40 and NCEP1 are shown here to be reliable back until at least 1970 and 1958, respectively, where station observations are available. Other validations [e.g., *Renwick*, 2004; *Sterl*, 2004] demonstrate the successes of the reanalyses in the Southern Hemisphere. In the NH, the skill of the reanalyses is even of higher quality than in the SH [e.g., *Bromwich and Wang*, 2005] throughout the year back until 1958. Thus there are many uses for the reanalyses despite the deficiencies mentioned here. Nonetheless, one must be aware of these problems and proceed with caution by comparing the reanalysis results with available observations, so that spurious biases in the reanalyses will not be misinterpreted [*Bengtsson et al.*, 2004c].

[40] **Note added in proof.** As part of the planning for the NASA Modern Era Retrospective-Analysis for Research and Applications (MERRA) global reanalysis (M. Bosilovich, personal communication, 2006), the temporal variation in zonal mean precipitation has been examined for ERA-40 and JRA-25, 1979–2001. JRA-25 has an abrupt decrease in forecast precipitation in the 40°–60° latitude band in both hemispheres that coincides with the start of SSM/I assimilation in 1987. It is much more pronounced over the Southern Ocean where assimilated SSM/I precipitable water amounts could be expected to have a major impact on the forecast precipitation.

[41] **Acknowledgments.** The authors would like to thank SCAR for providing funding for the workshop on the reanalyses in the high latitudes and for partial publication expenses. Data for NCEP1 and NCEP2 were obtained from the National Weather Service Climate Prediction Center reanalysis project (available online at http://www.cpc.ncep.noaa.

gov/products/wesley/reanalysis.html). ERA-40 reanalysis data were obtained from the University Corporation for Atmospheric Research data support section (see online at http://dss.ucar.edu, and the JRA-25 data were obtained directly from the project website, http://www.jreap.org. This research for D. H. Bromwich and R. Fogt was funded in part by NSF grant OPP-0337948, UCAR subcontract SO1-22961, and NOAA grant UAF04-0047, while research for J. E. Walsh was funded by NOAA grant NA17RJ1224 and DOE grant DESG-0206-ER64251. This is contribution 1351 of the Byrd Polar Research Center.

References

Adler, R. F., et al. (2003), The Version 2 Global Precipitation Climatology Project (GPCP) Monthly Precipitation Analysis (1979–present), *J. Hydrometeorol.*, *4*, 1147–1167.

Andersson, E., et al. (2005), Assimilation and modeling of the atmospheric hydrological cycle in the ECMWF forecasting system, *Bull. Am. Meteorol. Soc.*, *86*, 387–402.

Baldwin, M. P. (2001), Annular modes in global daily surface pressure, *Geophys. Res. Lett.*, *28*, 4115–4118.

Bengtsson, L., K. I. Hodges, and S. Hagemann (2004a), Sensitivity of large scale analyses to humidity observations and its impact on the global water cycle and tropical and extratropical weather systems in ERA40, *Tellus, Ser. A*, *56*, 202–217.

Bengtsson, L., K. I. Hodges, and S. Hagemann (2004b), Sensitivity of the ERA40 reanalysis to the observing system: determination of the global atmospheric circulation from reduced observations, *Tellus, Ser. A*, *56*, 456–471.

Bengtsson, L., S. Hagemann, and K. I. Hodges (2004c), Can climate trends be calculated from reanalysis data?, *J. Geophys. Res.*, *109*, D11111, doi:10.1029/2004JD004536.

Bromwich, D. H., and R. L. Fogt (2004), Strong trends in the skill of the ERA-40 and NCEP-NCAR reanalyses in the high and middle latitudes of the Southern Hemisphere, 1958–2001, *J. Clim.*, *17*, 4603–4619.

Bromwich, D. H., and S.-H. Wang (2005), Evaluation of the NCEP-NCAR and ECMWF 15- and 40-yr reanalyses using rawinsonde data from two independent Arctic field experiments, *Mon. Weather Rev.*, *133*, 3562–3578.

Bromwich, D. H., A. N. Rogers, P. Kållberg, R. I. Cullather, J. W. C. White, and K. J. Kreutz (2000), ECMWF analyses and reanalyses depiction of ENSO signal in Antarctic precipitation, *J. Clim.*, *13*, 1406–1420.

Bromwich, D. H., S.-H. Wang, and A. J. Monaghan (2002), ERA-40 representation of the Arctic atmospheric moisture budget, in *ECMWF Workshop on Reanalysis*, *ECMWF Re-Analysis Proj. Rep. Ser. 3*, pp. 287–298, Eur. Cent. for Medium-Range Weather Forecasts, Reading, UK.

Bromwich, D. H., Z. Guo, L. Bai, and Q.-S. Chen (2004), Modeled Antarctic precipitation. part I: Spatial and temporal variability, *J. Clim.*, *17*, 427–447.

Crochet, P. (2007), A study of regional precipitation trends in Iceland using ERA-40 reanalyses, *J. Clim*, in press.

Cullather, R. I., D. H. Bromwich, and M. C. Serreze (2000), The atmospheric hydrologic cycle over the Arctic basin from reanalyses. part I: Comparison with observations and previous studies, *J. Clim.*, *13*, 923–937.

Déry, S. J., and E. F. Wood (2004), Teleconnection between the Arctic Oscillation and Hudson Bay river discharge, *Geophys. Res. Lett.*, *31*, L18205, doi:10.1029/2004GL020729.

Fogt, R. L., and D. H. Bromwich (2006), Decadal variability of the ENSO teleconnection to the high latitude South Pacific governed by coupling with the Southern Annular Mode, *J. Clim.*, *19*, 979–997.

Francis, J. A. (2002), Validation of reanalysis upper-level winds in the Arctic with independent rawinsonde data, *Geophys. Res. Lett.*, *29*(9), 1315, doi:10.1029/2001GL014578.

Gibson, J. K., P. Kållberg, S. Uppala, A. Hernandez, A. Nomura, and E. Serrano (1997), ERA Description, *ECMWF Re-analysis Proj. Rep. Ser.*, part 1, 72 pp., Eur. Cent. for Medium-Range Weather Forecasts, Reading, UK.

Gong, D., and S. Wang (1999), Definition of Antarctic oscillation index, *Geophys. Res. Lett.*, *26*, 459–462.

Hanna, E., T. Jónsson, and J. E. Box (2004), An analysis of Icelandic climate since the nineteenth century, *Int. J. Climatol.*, *24*, 1193–1210.

Hines, K. M., D. H. Bromwich, and G. J. Marshall (2000), Artificial surface pressure trends in the NCEP-NCAR reanalysis over the Southern Ocean and Antarctica, *J. Clim.*, *13*, 3940–3952.

Hodges, K. I., B. J. Hoskins, J. Boyle, and C. Thorncroft (2003), A comparison of recent reanalysis datasets using objective feature tracking: Storm tracks and tropical easterly waves, *Mon. Weather Rev.*, *131*, 2012–2037.

Hodges, K. I, B. J.. Hoskins, J. Boyle, and C. Thorncroft (2004), Corrigendum, *Mon. Weather Rev.*, *132*, 1325–1327.

Hoskins, B. J., and K. I. Hodges (2002), New perspectives on the Northern Hemisphere winter storm tracks, *J. Atmos. Sci.*, *59*, 1041–1061.

Hoskins, B. J., and K. I. Hodges (2005), A new perspective on Southern Hemisphere storm tracks, *J. Clim.*, *18*, 4108–4129.

Ishii, M., A. Shouji, S. Sugimoto, and T. Matsumoto (2005), Objective analyses of sea-surface temperature and marine meteorological variables for the 20th century using ICOADS and the Kobe collection, *Int. J. Climatol.*, *25*, 865–879.

Kalnay, E., et al. (1996), The NCEP-NCAR 40 year reanalysis project, *Bull. Am. Meteorol. Soc.*, *77*, 437–471.

Kanamitsu, M., W. Ebisuzaki, J. Woollen, S. K. Yang, J. J. Hnilo, M. Fiorino, and G. L. Potter (2002), NCEP-DOE AMIP-II reanalysis (R-2), *Bull. Am. Meteorol. Soc.*, *83*, 1631–1643.

Kidson, J. W. (1999), Principal modes of Southern Hemisphere low frequency variability obtained from NCEP-NCAR reanalyses, *J. Clim.*, *12*, 2808–2830.

Kistler, R., et al. (2001), The NCEP-NCAR 50-year reanalysis: Monthly means CD-ROM and documentation, *Bull. Am. Meteorol. Soc.*, *82*, 247–267.

L'Heureux, M. L., and D. W. J. Thompson (2006), Observed relationship between the El Niño-Southern Oscillation and the extratropical zonal-mean circulation, *J. Clim.*, *19*, 276–287.

Marshall, G. J. (2002), Trends in Antarctic geopotential height and temperature: A comparison between radiosonde and NCEP-NCAR reanalysis data, *J. Clim.*, *15*, 659–674.

Marshall, G. J. (2003), Trends in the Southern Annular Mode from observations and reanalyses, *J. Clim.*, *16*, 4134–4143.

Marshall, G. J., and S. A. Harangozo (2000), An appraisal of NCEP/NCAR reanalysis MSLP data viability for climate studies in the South Pacific, *Geophys. Res. Lett.*, *27*, 3057–3060.

Monaghan, A. J., D. H. Bromwich, and S.-H. Wang (2006), Recent trends in Antarctic snow accumulation from polar MM5 simulations, *Philos. Trans. R. Soc., Ser. A*, *364*, 1683–1708.

Onogi, K., et al. (2006), JRA-25: Japanese 25-year re-analysis, *Q. J. R. Meteorol. Soc.*, *131*, 3259–3268.

Raphael, M. N. (2004), A zonal wave 3 index for the Southern Hemisphere, *Geophys. Res. Lett.*, *31*, L23212, doi:10.1029/2004GL020365.

Renwick, J. A. (2004), Trends in the Southern Hemisphere polar vortex in NCEP and ECMWF reanalyses, *Geophys. Res. Lett.*, *31*, L07209, doi:10.1029/2003GL019302.

Richman, M. B. (1986), Rotation of principal components, *J. Climatol.*, *6*, 293–335.

Schubert, S. D., R. B. Rood, and J. Pfaendtner (1993), An assimilated dataset for Earth science applications, *Bull. Am. Meteorol. Soc.*, *74*, 2331–2342.

Serreze, M. C. (1995), Climatological aspects of cyclone development and decay in the Arctic, *Atmos. Ocean*, *33*, 1–23.

Serreze, M. C., and C. M. Hurst (2000), Representation of mean Arctic precipitation from NCEP-NCAR and ERA reanalyses, *J. Clim.*, *13*, 182–201.

Serreze, M. C., F. Carse, R. G. Barry, and J. C. Rogers (1997), Icelandic low cyclone activity: Climatological features, linkages with the NAO, and relationships with recent changes in the Northern Hemisphere circulation, *J. Clim.*, *10*, 453–464.

Serreze, M. C., J. R. Key, J. E. Box, J. A. Maslanik, and K. Steffen (1998), A new monthly climatology of global radiation for the Arctic and comparisons with NCEP-NCAR reanalysis and ISCCP-C2 fields, *J. Clim.*, *11*, 121–136.

Serreze, M. C., M. P. Clark, and D. H. Bromwich (2003), Monitoring precipitation over the Arctic terrestrial drainage system: Data requirements, shortcomings, and applications of atmospheric reanalysis, *J. Hydrometerol.*, *4*, 387–407.

Serreze, M. C., A. P. Barrett, and F. Lo (2005), Northern high-latitude precipitation as depicted by atmospheric reanalyses and satellite retrievals, *Mon. Weather Rev.*, *133*, 3407–3430.

Serreze, M. C., A. P. Barrett, A. G. Slater, R. A. Woodgate, K. Aagaard, R. B. Lammers, M. Steele, R. Moritz, M. Meredith, and C. M. Lee (2006), The large-scale freshwater cycle of the Arctic, *J. Geophys. Res.*, *111*, C11010, doi:10.1029/2005JC003424.

Serreze, M. C., A. P. Barrett, A. G. Slater, M. Steele, J. Zhang, and K. E. Trenberth (2007), The large-scale energy budget of the Arctic, *J. Geophys. Res.*, doi:10.1029/2006JD008230, in press.

Sterl, A. (2004), On the (in)homogeneity of reanalysis products, *J. Clim.*, *17*, 3866–3873.

Sturaro, G. (2003), A closer look at the climatological discontinuities present in the NCEP/NCAR reanalysis temperature due to the introduction of satellite data, *Clim. Dyn.*, *21*, 309–316.

Su, F., J. C. Adam, K. E. Trenberth, and D. P. Lettenmaier (2006), Evaluation of surface water fluxes of the pan-Arctic land region with a land surface model and ERA-40 reanalysis, *J. Geophys. Res.*, *111*, D05110, doi:10.1029/2005JD006387.

Tennant, W. (2004), Considerations when using pre-1979 NCEP/NCAR reanalyses in the Southern Hemisphere, *Geophys. Res. Lett.*, *31*, L11112, doi:10.1029/2004GL019751.

Thompson, D. W., J. M. Wallace, and G. C. Hegerl (2000), Annular modes in the extratropical circulation. part II: Trends, *J. Clim.*, *13*, 1018–1036.

Trenberth, K. E., and L. Smith (2005), The mass of the atmosphere: A constraint on global analyses, *J. Clim.*, *18*, 864–875.

Trenberth, K. E., D. P. Stepaniak, and L. Smith (2005), Interannual variability of patterns of atmospheric mass distribution, *J. Clim.*, *18*, 2812–2825.

Turner, J., T. Lachlan-Cope, S. Colwell, and G. J. Marshall (2005), A positive trend in western Antarctic Peninsula precipitation over the last 50 years reflecting regional and Antarctic-wide atmospheric circulation changes, *Ann. Glaciol.*, *41*, 85–91.

Uppala, S. M., et al. (2005), The ERA-40 reanalysis, *Q. J. R. Meteorol. Soc.*, *131*, 2961–3012, doi:10.1256/QJ.04.176.

van de Berg, W. J., M. R. van den Broeke, C. H. Reijmer, and E. van Meijgaard (2005), Characteristics of Antarctic surface mass balance, 1958–2002, using a regional atmospheric climate model, *Ann. Glaciol.*, *41*, 97–104.

van de Berg, W. J., M. R. van den Broeke, C. H. Reijmer, and E. van Meijgaard (2006), Reassessment of the Antarctic surface mass balance using calibrated output of a regional atmospheric climate model, *J. Geophys. Res.*, *111*, D11104, doi:10.1029/2005JD006495.

Vaughan, D. G., J. L. Bamber, M. Giovinetto, J. Russell, and A. P. R. Cooper (1999), Reassessment of net surface mass balance in Antarctica, *J. Clim.*, *12*, 933–946.

Walsh, J. E., and W. L. Chapman (1998), Arctic cloud-radiation-temperature associations in observational data and atmospheric reanalyses, *J. Clim.*, *11*, 3030–3045.

Wang, X. L., V. R. Swail, and F. W. Zwiers (2006), Climatology and changes of extratropical cyclone activity: Comparison of ERA-40 with NCEP-NCAR reanalysis for 1958–2001, *J. Clim.*, *19*, 3145–3166.

D. H. Bromwich and R. L. Fogt, Polar Meteorology Group, Byrd Polar Research Center, 1090 Carmack Road, 108 Scott Hall, Columbus, OH 43210, USA. (bromwich.1@osu.edu)

K. I. Hodges, Environmental Systems Science Center, University of Reading, Harry Pitt Building, 3 Earley Gate, Whiteknights, P.O. Box 238, Reading RG6 6AL, UK.

J. E. Walsh, International Arctic Research Center, University of Alaska-Fairbanks, 930 Koyukuk Drive, P.O. Box 757340, Fairbanks, AK 99775-7340, USA.